Postprint of: Nitka M., Tejchman-Konarzewski A., Kozicki J., Leśniewska D., DEM analysis of micro-structural events within granular shear zones under passive earth pressure conditions, GRANULAR MATTER, Vol. 17, Iss. 3 (2015), pp. 325-343

DEM analysis of micro-structural events within granular shear zones under passive earth pressure conditions

M. Nitka[1], J. Tejchman[1], J. Kozicki[1] and D. Leśniewska[2]

[1]Faculty of Civil and Environmental Engineering

Gdańsk University of Technology, Gdańsk, Poland

micnitka@pg.gda.pl, tejchmk@pg.gda.pl, jkozicki@pg.gda.pl

[2] Faculty of Civil Engineering, Environmental and Geodetic Sciences

Koszalin University of Technology

danuta.lesniewska@tu.koszalin.pl

Abstract:

Shear zones in initially medium dense cohesionless sand for quasi-static earth pressure problem of a small-scale retaining wall were analysed with a discrete element method (DEM) using spheres with contact moments. The passive sand failure for a very rough retaining wall undergoing horizontal translation was discussed. The DEM calculations were carried out with the different mean grain diameter. Micro-structural events appearing within granular shear zones such as: vortices, force chains, vortex structures and local void ratio fluctuations were investigated. Special attention was laid on a vortex - force chain correlation and the frequency of the vortex appearance. The calculated geometry of shear zones was compared with experimental results of laboratory model tests analyzed using the DIC. DEM demonstrated its ability to describe the geometry of shear localization in sand behind the retaining wall and to follow the evolution of micro-structure in granular shear zones.

Keywords: DEM, granular material, micro-polar hypoplasticity, micro-structure evolution, retaining wall, shear zone

1. Introduction

Earth pressure on retaining walls is one of the soil mechanics classical problems. It is also the example of an experimental arrangement which can be employed to study the basic features of granular materials, as it produces a relatively simple pattern of localized deformation at boundary conditions naturally allowing for principal stress rotations. Strain localization in the case of model tests on a retaining wall moving in a passive mode is easy to observe at relatively large wall displacements but becomes quite a challenge within a small displacements rang, when the passive

earth pressure starts to develop from the at rest condition. The experimental observations coming from historical small-scale model tests on walls (i.e. Roscoe [1]) provide a basis to simple limit analysis models, still used in the geotechnical practice to estimate earth pressures. The models are usually based on an a priori accepted failure mechanisms, concluded from experimental observations at a large deformation stage,and the results of their predictions depend on this mechanisms' closeness to the reality. Some recent experimental papers [2], [3] revealed that the progress of shear localization behind retaining walls can be much more complex than it could be imagined, before methods such as e.g. the digital image correlation (DIC) technique were introduced into the experimental soil mechanics. Some other recently developed numerical methods (like DEM) can grossly support experimental methods, especially at a grain scale which is out of the reach for experimental testing methods, even in the case of small geotechnical models. The necessary condition to substitute physical models with DEM is that the latter must be calibrated and verified using real data. For these data types which are not easily available from experiments (like the evolution of the earth pressure with the wall displacement), the calibrated FE simulations may provide the missing information. Taking into account the above remarks, the purpose of this paper is twofold: 1) to calibrate the DEM model of a small-scale passive earth pressure problem to obtain a realistic pattern of shear zones and 2) to use DEM to investigate the collective micro-behaviour of grains inside shear zones.

One especially interesting feature characterizing shear zones within granular materials, namely so-called vortex structures, reported by several researchers (e.g. [4]-[6]) can be studied using the same DEM model. It is difficult to say at this stage of research whether vortex structures have any significant impact on earth pressure values and how they could be taken into account in earth pressure calculations. The reason is that the mechanisms ruling the creation and diminishing of vortices are not fully recognized yet. As there are quite contradictory opinions on the topic in the literature, based on physical experiments, this paper tries to find out using the passive earth pressure DEM model which physical phenomenon may govern the existence of vortex structures in granular materials. Several other characteristic micro-structural events occurring within shear zones at the grain-level were also studied, such as: changes in force chains, local void ratio fluctuations and local strain non-uniformities.

This paper is a continuation of the previous research presented by Widulinski et al. [2], where the capability of DEM to describe patterns of shear zones in sand placed behind rigid and very rough retaining wall undergoing passive and active movements (horizontal translation, rotation about the top and rotation about the toe) was proved. That paper was focused on a direct comparison between

discrete, finite element and experimental results at the global level, i.e. with respect to the geometry of shear zone patterns and load-displacement diagrams. In the present paper, more attention was paid to micro-structural changes within granular shear zones appearing in sand during horizontal wall translation. The major contribution of the manuscript is the numerical evidence of the correlation between a location of vortex structures and force chain breakage and estimation of the frequency of vortices appearance within a shear zone.

The paper is organized as follows: Section 2 summarizes the experimental results concerning geometry of shear zones during passive wall translation. Section 3 contains the DEM model description. Section 4 includes the detailed analysis of the evolution of micro-structure within shear zones and Conclusions are given in Section 5.

2. Experimental shear zone patterns

Figure 1 shows shear zones observed at final stages of small-scale passive mode experiments on initially dense sand during horizontal rigid wall translation (from left to right), revealed by means of x-rays (Figs.1a and 1b) and DIC (Fig.1c) [7]-[9]. The experiments performed are the typical 2D boundary value problems, i.e. the effect of the specimen depth on the shear zone pattern is negligible [8], [9].

a)

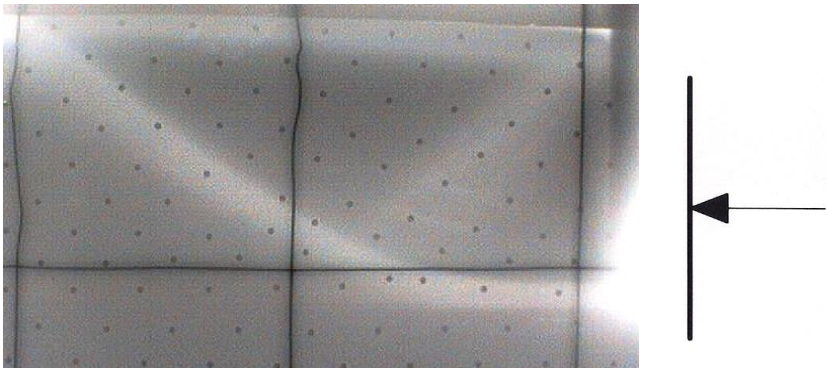

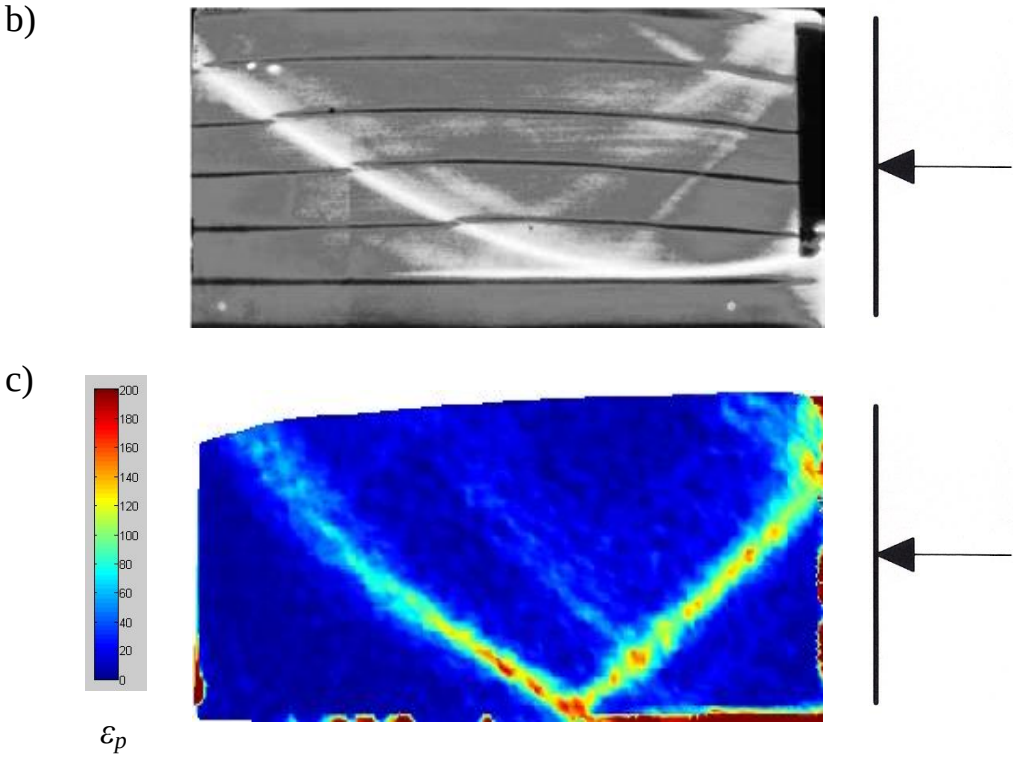

Fig. 1 Shear zones observed in experiments on initially dense sand during passive mode horizontal wall translation:
a X-ray image for 'Leighton Buzzard' sand (mean grain diameter d_{50} = 0.9mm and wall height h = 0.33 m) [7],
b X-ray image for 'Karlsruhe' sand (d_{50} = 0.50mm and h = 0.175 m) [8] and
c DIC image for Borowiec' sand (d_{50} = 0.8mm and h = 0.23 m) [9] (ε_p—shear strain)

In all three experiments (Fig.1a-c), a distinct single main shear zone started from the toe of the wall to the free boundary and was accompanied by some fainter, secondary radial shear zones, propagating from the top of the wall. The main shear zone in each case included an almost horizontal part at the beginning of its course, forming a characteristic 'fork' with the curved part at some distance from the wall. The radial shear zones seem to 'fill in' the area between two limiting straight lines (that is best visible in Fig.1b, but also discernible in Figs.1a and 1c). In the last case, the right limiting line is obviously much more developed than the left one. In addition, traces of some not fully developed shear zones can be observed in Fig.1 - one emerging slightly below the top of the wall in the right up corner of the specimen and propagating to the free boundary (Figs.1b and 1c) and the other in the middle of the specimen, parallel to the main shear zone and propagating also to the free boundary (Fig.1c). These zones appear slightly later than the main and the radial ones.

Shear zones can be recognized on radiographs due to density decrease (dilatancy), accompanying shear deformation of granular materials (brighter zones in Figs.1a and 1b). It means that radiographs show only localized volume changes but not shear strains. The digital photography and

DIC method can provide both volumetric and shear strains – the latter, calculated for the test on 'Borowiec' sand, are shown in Fig.1c.

3. Discrete Element Method

In numerical analyses using DEM, the mechanical response of geomaterials is governed by interactions at contacts between constituent particles and between particles and boundaries, which are responsible for the emergent complexity of phenomena occurring in these materials [10]. To simulate the behaviour of sand, the three-dimensional spherical discrete model YADE was used which takes into account the so-called soft-particle approach (i.e. the model allows for particle deformation which is represented as an overlap of particles) [11]. In the paper, only spherical elements were used. To simulate the sand grain's roughness, additional moments were introduced into the 3D model, which were transferred through contacts and resisted particle rotations [12]. In this way, grains were in contact with their neighbours through a certain contact surface [13]-[15]. We used exclusively spherical particles and simulated the influence of the contact flatness, and thus the influence of the grain shape by assuming bending moments and bending stiffnesses at particle contacts. This approach has one big advantage [16]: the computation time is significantly shortened (calculations on spheres with contact moments are 3-5 times faster than those using complex clumps). A simple linear elastic normal contact model was assumed to simulate average various contact features possible in real sand (Fig.2). No forces were transmitted when grains were separated (tension was not allowed). The unloading was purely elastic (Fig.2C). The elastic contact constants E_c nad ν_c were specified from the experimental triaxial compression test and could be related to the global modulus of elasticity of the grain material and its Poisson's ratio [17]. Therefore the elastic constants of the grain contact in our model do not correspond to the elastic constants of the spheres' material in the Hertz-Mindlin-Deresiewicz interaction law [18], [19] which is the exact elastic solution (e.g. the normal stiffness is several times larger than the mean normal stiffness of the spherical grain material). Although the non-linear contact law is more realistic, a linear contact law provides similar results with the significantly reduced computation time [20] and therefore was used in the present simulations. To dissipate excessive kinetic energy in the discrete system, a simple local non-viscous damping scheme was adopted by assuming a slight change of forces and moment due to damping (the forces and moment were multiplied by the damping parameter α) to obtain this change [10]).

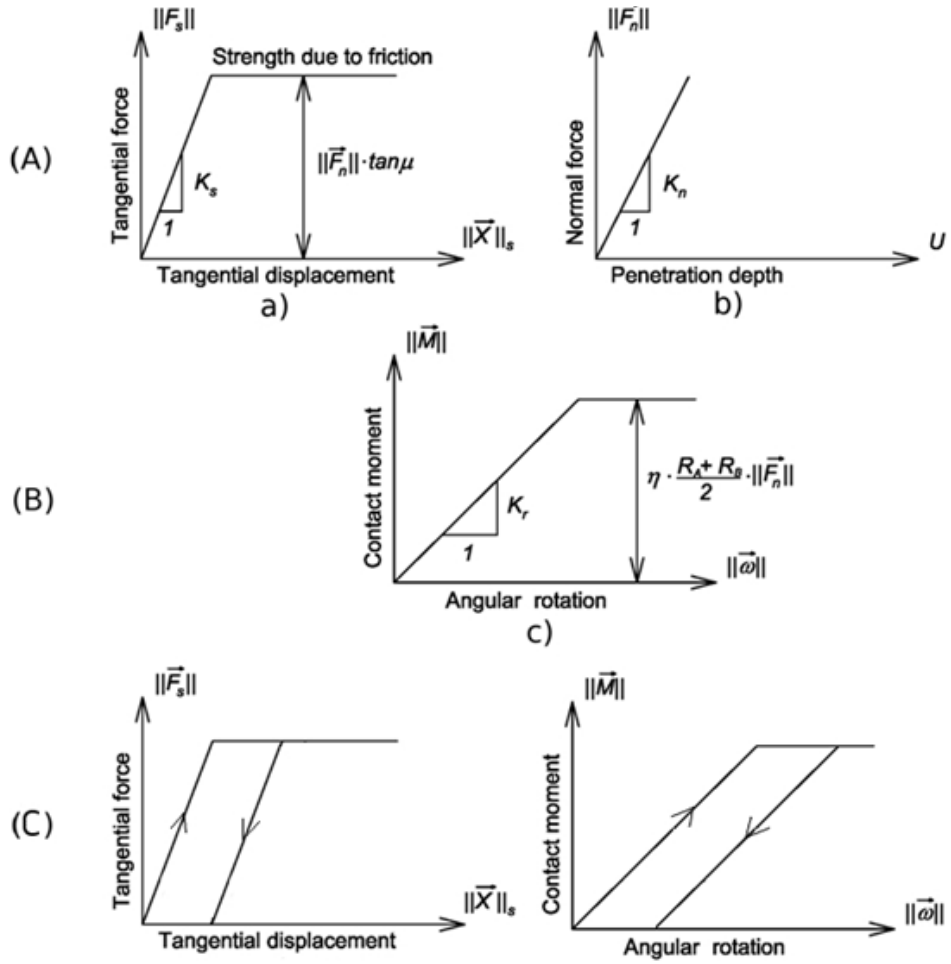

Fig. 2 Mechanical response of linear contact model without (**A**) and with contact moments (**A**+**B**): **a** tangential contact model, **b** normal contact model and **c** rolling contact model and (**C)** loading and unloading path (tangential and rolling contact) wherein: F_s - tangential force vector between elements, F_n - normal force vector between element, M - contact moment vector, K_s - tangential stiffness, K_n - normal stiffness, K_r - rolling stiffness, U - penetration depth,_X_s - tangential displacement vector, _ω—angular rotationvector, μ—inter-particle frictionangle, η—limit rolling coefficient [19,20]

The five main local material parameters are necessary in our discrete simulations [16], [20]: E_c (modulus of elasticity of the grain contact), ν_c (Poisson's ratio of the grain contact), μ (inter-particle friction angle), β (rolling stiffness coefficient) and η (limit rolling coefficient). In addition, a particle radius R, particle mass density ρ and numerical damping parameter α are required. The material parameters of DEM ($E_c, \nu_c, \mu, \beta, \eta$ and α) were calibrated using the corresponding axisymmetric triaxial laboratory test results on Karlsruhe sand by Wu [21]. The index properties of Karlsruhe sand are: mean grain diameter d_{50}=0.50 mm, grain size between 0.08 mm and 1.8 mm, uniformity coefficient U_c=2, maximum specific weight γ_d^{max}=17.4 kN/m^3, minimum void ratio e_{min}=0.53, minimum specific weight γ_d^{min}=14.6 kN/m^3 and maximum void ratio e_{max}=0.84. The sand grains are classified as sub-rounded/sub-angular.

4. DEM modelling results of passive earth pressure model tests

The discrete 2D calculations were performed for a sand body of 0.40 m length and 0.20 m height in order to compare them with the experiments (Fig.1b). The vertical retaining wall and the bottom of the granular specimen were assumed to be stiff and very rough, i.e. there was no relative displacement along vertical and bottom surface. Since the effect of the specimen depth in out of plane direction turned out to be almost negligible during direct shearing of spheres with contact moments [20], in order to significantly accelerate simulations, the DEM calculations were performed mainly with the specimen depth equal to the grain size d (i.e. one layer of spheres a perpendicular plane was simulated only) and the calculations were carried out as for cylinders (instead of spheres).

The spheres of three different mean grain diameters were employed for simulations, characterized by a linear grain size distribution (GSD): d_{50}=5.0 mm (grain size varying between 2.5-7.5 mm, 2'600 spheres sample), d_{50}=2.0 mm (grain size range 1-3 mm, 15'600 spheres sample) and d_{50}=1.0 mm (grain size range 0.5-1.5 mm, 62'600 spheres sample). The choice of the grain sizes was again limited by the computational time cost. The initial void ratio of sand, obtained by generating random spheres above a box and then allowing them to fall down by gravity, was e_o=0.62 (similar as in the FEM calculations). The loading speed was slow enough to ensure that the numerical tests were conducted under quasi-static conditions; the calculated nominal inertial number (which quantifies the significance of dynamic effects) in the analyses was $I = \frac{\dot{\gamma} d_{50}}{\sqrt{\frac{P}{\rho}}} =$ 10^{-4} -10^{-5} ($\dot{\gamma}$ is the shear rate, P is the pressure and ρ is the density). The value $I < 10^{-3}$ corresponds to a quasi-static regime [22], [23]). The calculations were carried out using the following parameters [16]: E_c=0.3 GPa, v_c=0.3, μ=18°, β=0.7, η=0.4, ρ=2.55 g/cm^3 and a=0.08 for d_{50}=1 mm, 2 mm or 5 mm. The CPU computation time was about 14 days for d_{50}=2 mm and 30 days for d_{50}=1 mm, using PC 3 GHz. Other quasi-static calculations [16] have shown that the effect of the numerical damping parameter α is insignificant if $\alpha \leq 0.08$ (α=0.08 was assumed in this paper). The granular assembly was prepared by putting spheres of a random radius according to the grain distribution curve into a container 0.2 m×0.4 m×d_{50} [24]. Due to gravity, the spheres moved to the bottom wall and their arrangement became random. In order to obtain a desired low initial void ratio of e_o=0.62 with the grain overlapping, the inter-particle friction angle μ was stablished as 0° to exactly reproduce the target initial void ratio. The assembly was then allowed to settle to a state where the kinetic energy was negligible (below 10^{-8}) and the friction angle was set to μ=18°.

Figure 3 shows the evolution of the resultant normalized horizontal earth pressure force (earth pressure coefficient) $K_p=2E_h/(\gamma h^2 d_{50})$ versus the normalized horizontal wall displacement u/h (h=0.2 m - wall height, E_h – the horizontal force acting on the wall, γ=16.75 kN/m^3 - initial volumetric unit of sand) for 3 different sphere sizes from plane DEM simulation. The normalized horizontal earth pressure force evolves typically for initially dense granulates in biaxial compression, triaxial compression and shearing. The specimen exhibits on average the initial strain hardening up to the peak (u/h=0.03), followed by some softening before the common asymptote is reached. The force strongly fluctuates after the peak that can be attributed to the build-up and collapse of 'force chains' - the main carrier of stresses transferred within the granular assembly (see Section 4.3). For the larger spheres, the earth pressure coefficient K_p^{max} is higher than for the smaller ones: K_p^{max}=37 for d_{50}=5 mm, K_p^{max}=34 for d_{50}=2 mm and K_p^{max}=30 for d_{50}=1 mm. It can be thus anticipated that for d_{50}=0.5 mm (real sand), K_p^{max} should be about 25-27. The curve K=f(u/h) is of a similar character as the corresponding curve obtained by FEM [24]-[26], except for the lack of strong oscillations in FEM results. The calculated earth pressure coefficients are higher than the earth pressure coefficients obtained by a simple limit analysis calculations based on the assumption of one circular slip line (K_{pr}=11.3-25.8) or three straight slip lines (K_{pt}=13.4-23.7) constituting the failure mechanism of a retaining structure at $\delta=\varphi^p$=40°-45° (δ - wall friction angle between soil and structure, φ^p - internal friction angle of dense sand at peak, '*r*' rotation' and '*t*' – translation) [27]. It can be explained by the high initial density of sand and wall roughness, the scale effect resulting from the relatively high ratio between the mean grain diameter and wall height [24] and also the low stress level.

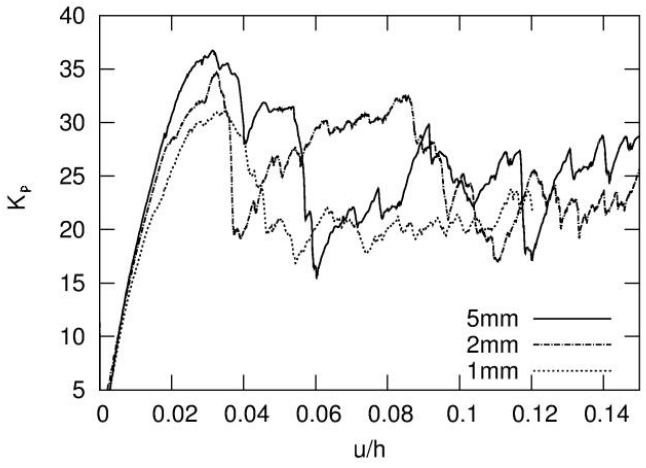

a)

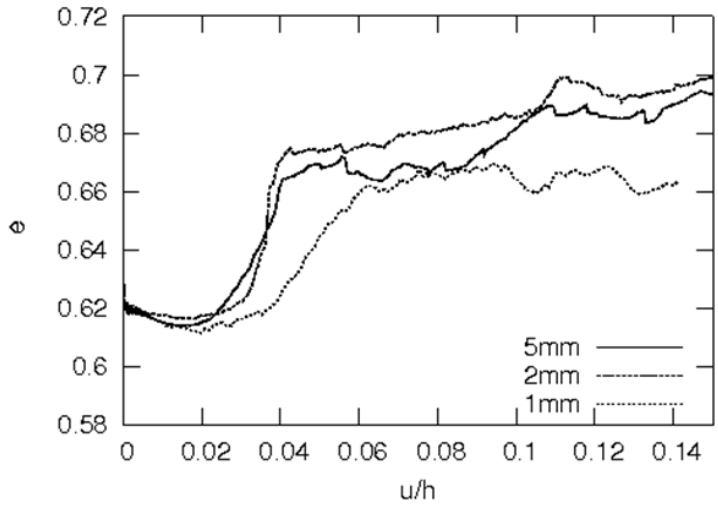

b)

Fig. 3 DEM results (passive case, translating wall): **a** evolution of resultant normalized horizontal earth pressure force $2Eh/(\gamma\, h2d_{50})$ versus normalized horizontal wall displacement u/h, **b** evolution of global void ratio e versus u/h (γ = 16.75 kN/m3, h = 0.2m, eo = 0.63, d_{50} = 1, 2 and 5 mm)

It comes from the evolution of the resultant (global) void ratio of the entire sand specimen that after some initial contractancy, the granular specimen is subjected to strong global dilatancy (u/h>0.1), also showing some fluctuations, but not as strong as in the case of the earth pressure coefficient (Fig.3b). The dilatancy for smaller spheres (d_{50}=1.0 mm) is lower than for the larger ones.

4.1 Distribution and evolution of sphere rotations

A typical particle configuration in the residual state (at u/h=0.15), showing in colour the distribution of single sphere rotations ω is presented in Fig.4 (red denotes the sphere rotation ω>+30^o and blue ω<-30^o, dark grey is related to the sphere rotation in the range 5^o≤ω≤30^o and light grey to the range -30^o≤ω≤-5^o, positive sign means clockwise rotation). All grains rotating within the range -5^o≤ω≤5^o are medium grey. Accepting such colour convention makes shear zones clearly observable (only particles within shear zones significantly rotate). As Fig.4 shows, there exists a clear grain separation regarding clockwise (red) and anticlockwise (blue) rotation – the vast majority of 'red grains' is located within the dominant shear zone, while the vast majority of 'blue grains' is placed within the secondary radial shear zone (however there exists also a small amount of blue grains within the 'red shear zone' and *vice versa*). Such a separation mechanism can be easily explained if one realizes that the wedge of granular material limited by the two shear zones moves upwards as a quasi-rigid body (not only in DEM simulation but also in reality – see Fig.1). If the wedge is replaced for simplicity by two planes sliding upwards on the medium of circulating grains (Fig.4d), it is obvious that the movement of two planes has to make grains lying along them to rotate in opposite directions. Such situation is possible only at final stages of deformation, when the contacts between grains within shear zones stop to exist.

Another general observation which can be made looking at Fig.4 (and especially at Fig.4c) is that there is a striking qualitative agreement between DEM simulations and real experiments of Fig.1 with respect to the geometry of main localized zones. It can be explained by the common base on which the numerical methods are founded - the general minimum energy principle, which may also well govern a choice that the real granular material makes. All experimental mechanisms of shear localization in Fig.1 are very similar - it may mean that for a given geometry of the problem this is an optimum way (requiring the smallest amount of energy) to deform granular materials. The main difference between Figs.4a-4c is related to the straight radial shear zone which appears at the top of the wall at certain stage of deformation and propagates to the specimen bottom - it is faintly visible in Fig.4a (the greatest grain diameter) and very clear in Figs.4b and 4c (d_{50}=1-2 mm). It seems its inclination to the vertical also depends on the mean grain diameter for u/h=0.15 - it is 30^o for d_{50}=2 mm and 50^o for d_{50}=1 mm. Except of the main shear zones, discussed above, there exist also in all three cases other faintly visible localized zones. The course of a dominant shear band marked by a large number of red grains in Figs.4a-4c does not seem to be affected by the grain diameter. The grain diameter obviously affects the width of strain localization but one must keep in mind that this value cannot be determined accurately, no matter which measure is used to visualize it. The assumption was met in this paper that the edges of a shear zone were defined by an arbitrarily chosen amount of the resultant grain rotation ω^f, namely by the condition $|\omega^f|>5^o$ (Figs.5a and 5b). The value of ω^f comes from the averaging of single sphere rotations over the small specimen area of $A_s=5d_{50}\times 5d_{50}$, by moving the area A_s by the $1\times d_{50}$ distance. Under this assumption, the thickness t_s of the main curved shear zone increases with increasing mean grain diameter d_{50} (Figs.4 and 5). Based on the distribution of the resultant grain rotation ω^c, the shear zone thickness measured along the cross section 'A-A' (Fig.5) at the residual state is: $t_s\approx$50 mm ($10\times d_{50}$) for d_{50}=5 mm, $t_s\approx$33 mm ($16\times d_{50}$) for d_{50}=2 mm and $t_s\approx$20 mm ($20\times d_{50}$) for d_{50}=1.0 mm. The width of the main shear zone grows in the certain range of deformation (u/h=0.02-0.11 for d_{50}=1.0 mm, Fig.6) and then reaches its maximum. The calculated mean inclination of the main curved shear zone to the horizontal is about 40^o (d_{50}=1-5 mm) is close to the experimental values of 35^o-40^o (Fig.1). The resultant grain rotation ω^f has its maximum in the mid-width of the shear zone (Fig.5). It is about 70^o (d_{50}=1.0 and 2.0 mm) and 45^o (d_{50}=5.0 mm) at u/h=0.15. Figure 5 suggests a parabolic distribution of ω^f across shear zone, the same as FEM calculations [24]. The maximum calculated single sphere rotation ω is about 75^o at u/h=0.15 (Fig.4). The displacement profile in the shear zone (Fig.6A) is similar to the profile obtained by FEM calculations [24].

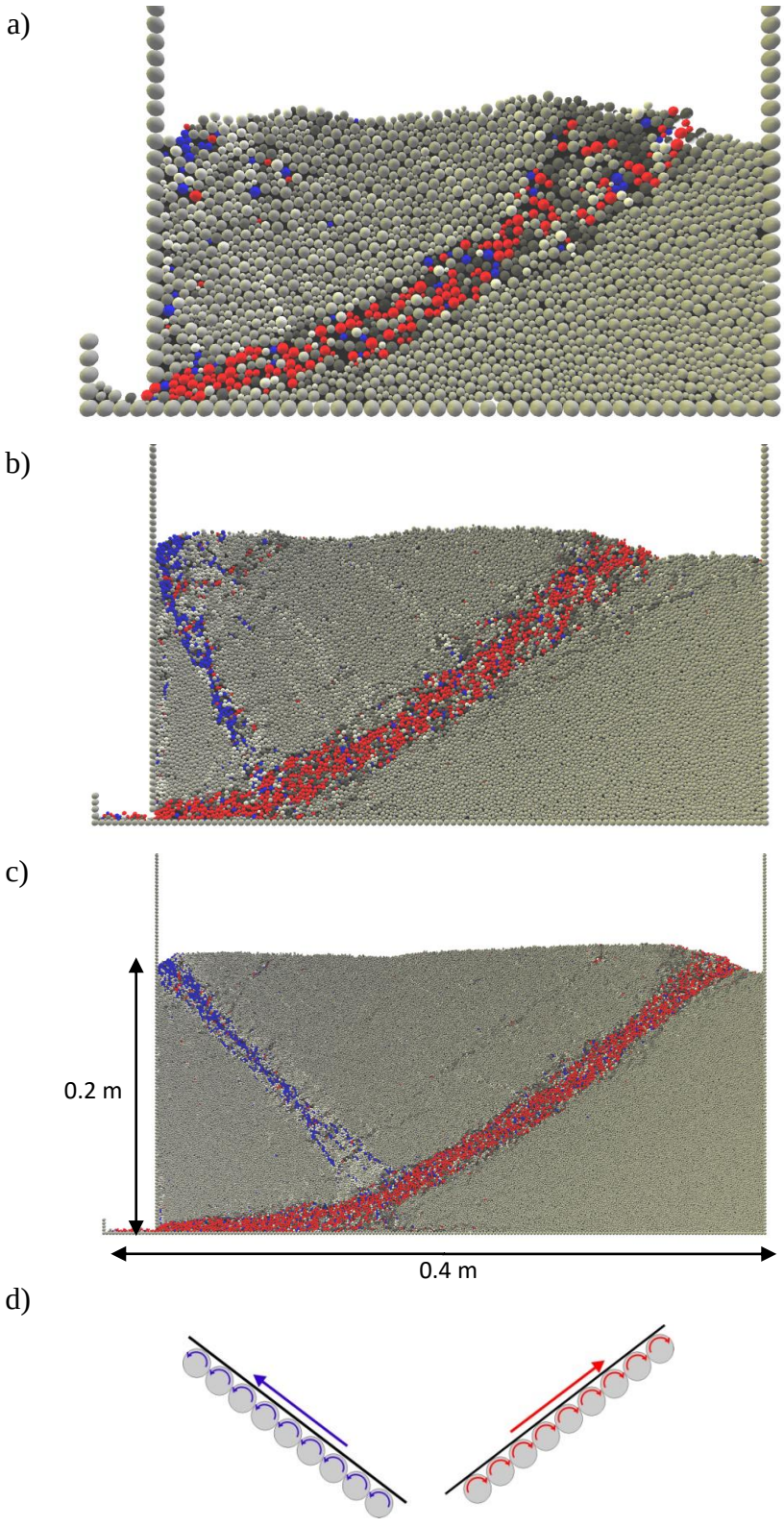

Fig. 4 Deformed granular body 0.2×0.4m^2 with distribution of rotation for initially medium dense sand (e_o = 0.62) from DEM at residual state of u/h = 0.15: **a** d_{50} = 5mm, **b** d_{50} = 2 mm, **c** d_{50} = 1mm (*red colour* denotes clockwise rotation$\omega > +30^\circ$, *blue colour* denotes anticlockwise rotation $\omega < -30^\circ$), **d** explanation for separation of clockwise and anticlockwise rotations within shear zones

4.2 Distribution and evolution of void ratio

The distribution of void ratio (averaged in the cell size A_s=5d_{50}×5d_{50}) across the main shear zone is also strongly non-uniform and also has its maximum along the centre-line (Figs.5c and 7). The void ratio alternates along the shear zone in a nearly periodic fashion as in biaxial compression tests analysed by DIC technique [28]. The specimen globally dilates within shear zones, however a local void ratio may also decrease (Fig.5c). Thus, local contractancy within shear zones is observed (Fig.5c). The maximum void ratio e in the main shear zone at the residual state is about 0.74 (Fig.5c) and is similar to the value obtained by FEM (e=0.78) [24]. Outside the shear zone the void ratio is within the range of e=0.63-0.65.

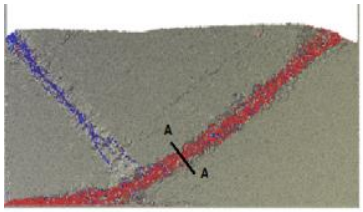

a)

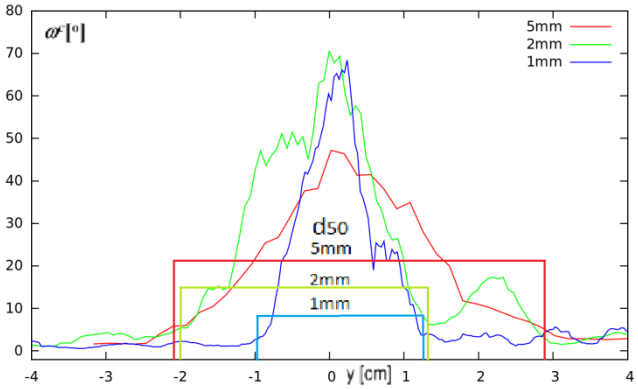

b)

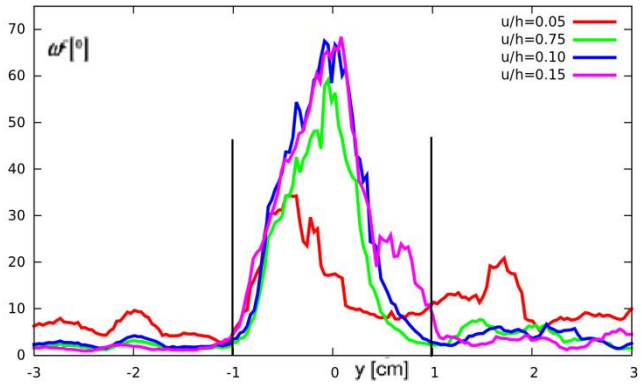

c)

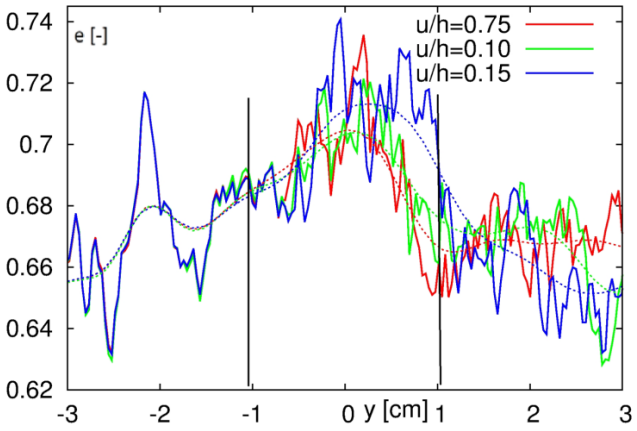

Fig. 5 DEM results (e_o = 0.62): **a** distribution of resultant grain rotation ω_c across curved shear zone width '*y*' in initially medium dense sand at residual state of *u*/*h* = 0.15 for different mean grain diameters d_{50} = 1–5mm, **b** distribution of resultant grain rotation ω_c against *u*/*h* (d_{50} = 1mm) and **c** distribution of void ratio *e* against *u*/*h* (d_{50} = 1mm) (*dotted line* corresponds to average values) across shear zone width '*y*' in initially medium dense sand (*vertical solid line* edges of shear zone)

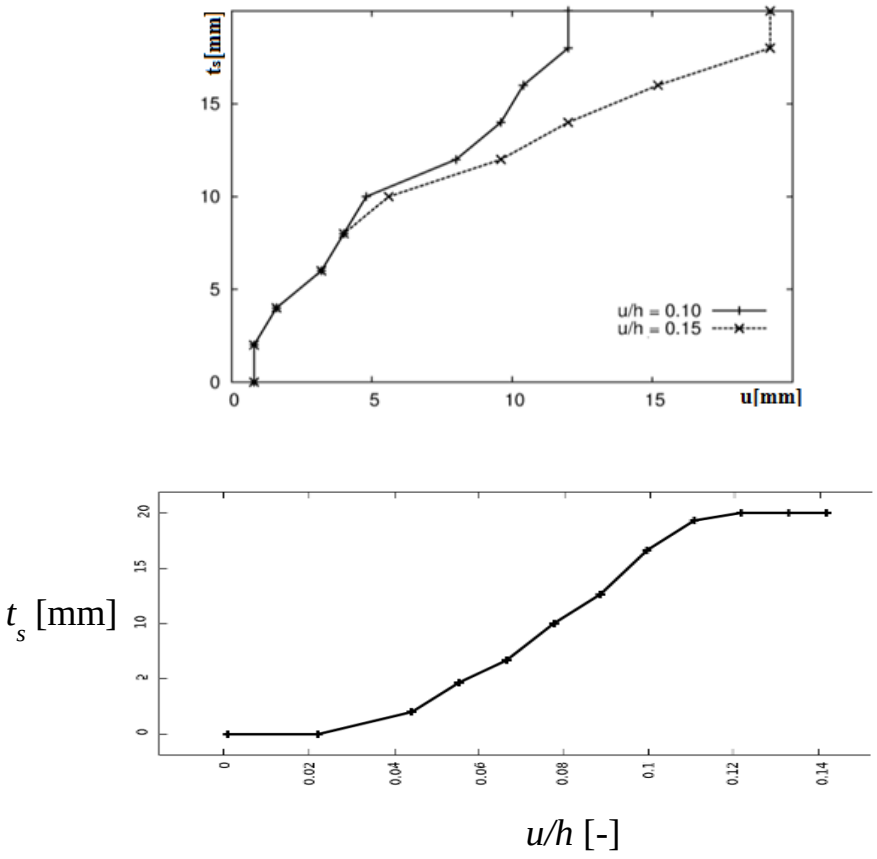

Fig. 6 DEM results (e_o = 0.62, d_{50} = 1.0mm): **A** displacement profile across shear zone width of 20 mm in mid-region of curved shear zone at: **a** *u*/*h* = 0.10 and **b** *u*/*h* = 0.15 and **B** the evolution of width of curved shear zone t_s at mid-length during horizontal normalized wall displacement *u*/*h*

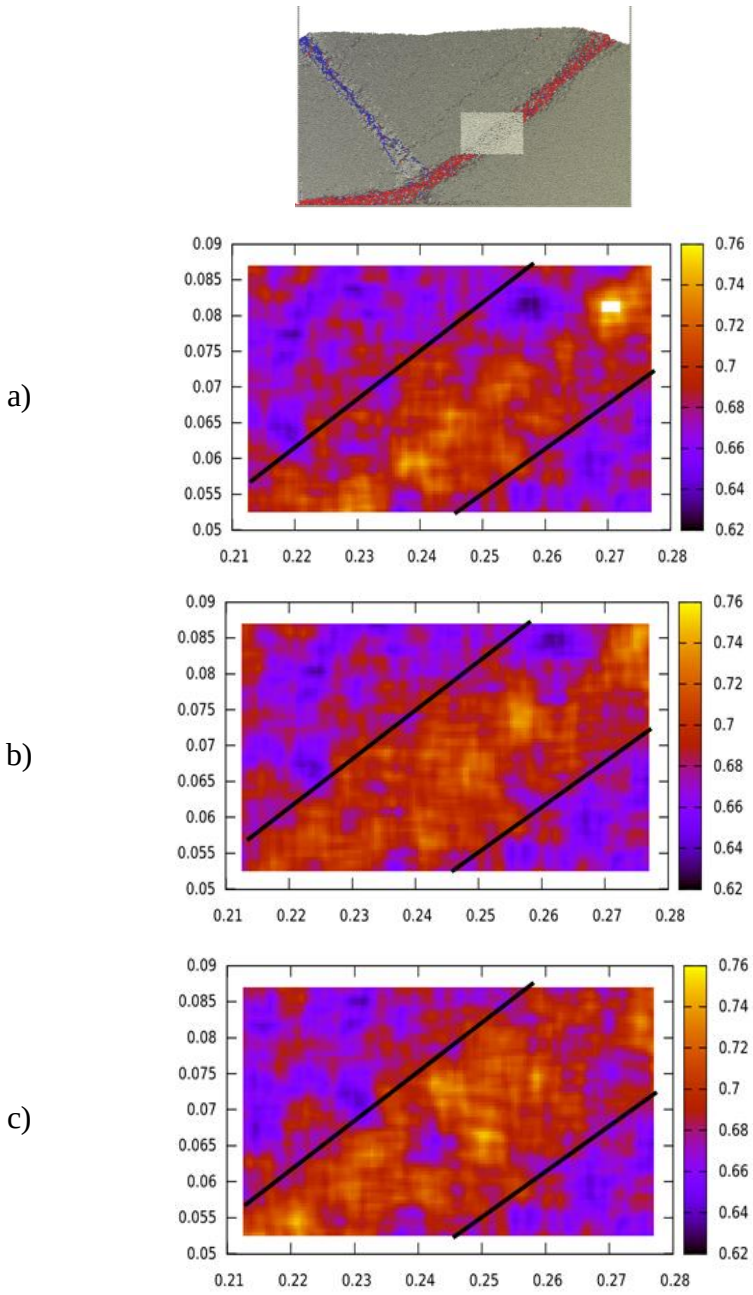

Fig. 7 DEM results: distribution of void ratio *e* in part of curved shear zone (e_o = 0.62, d_{50} = 1.0mm) for initially medium dense sand from DEM for different horizontal wall displacement: **a** *u*/*h* = 0.065, **b** *u*/*h* = 0.10 and **c** *u*/*h* = 0.15 (*vertical left axis* vertical co-ordinate, *vertical right axis* void ratio, *horizontal axis* horizontal co-ordinate, *solid lines* edges of shear zone)

4.3 Distribution and evolution of contact forces

Figure 8 shows the three stages of the main shear zone evolution seen through the contact force network: a) onset of shear localization, b) developing shear zone and c) shear zone fully developed. The location of the shear zone is indicated in Fig.8 by the dashed lines. The 'force chains' bearing loads greater than average are marked red and those loaded below the average are marked green. It can be seen from Fig.8 that the 'force network' becomes 'coarser' in the area of growing localized deformation.

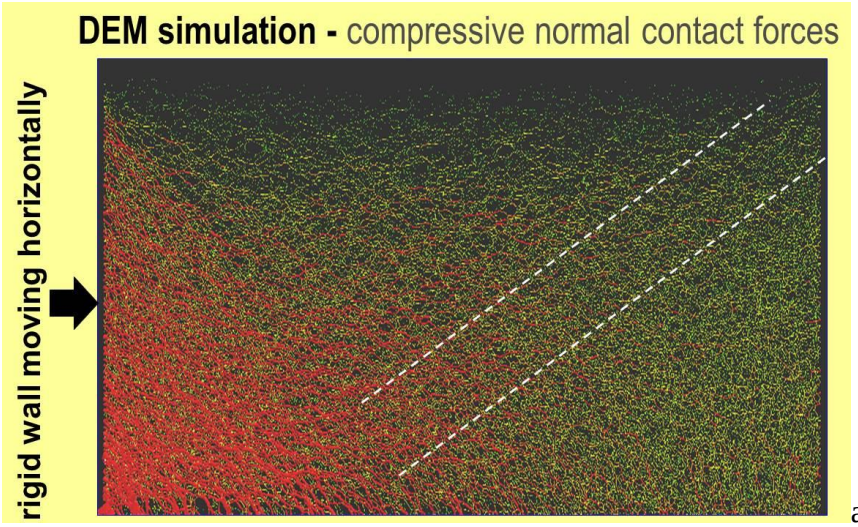

a)

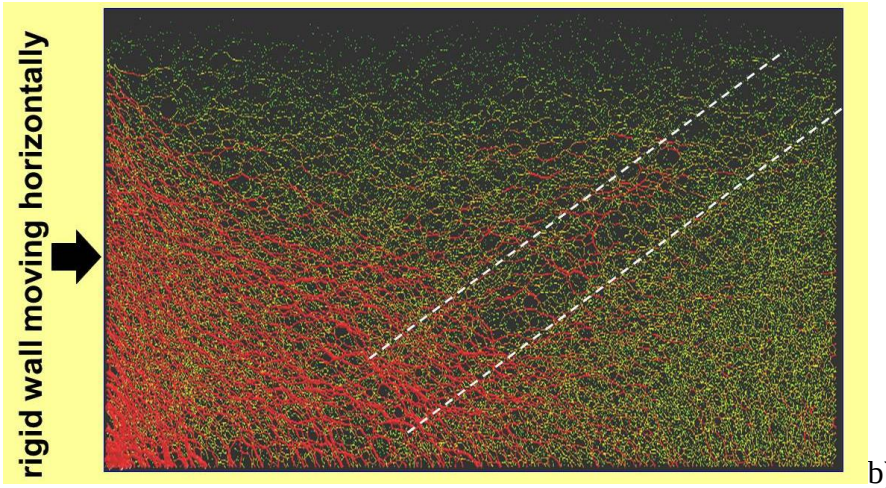

b)

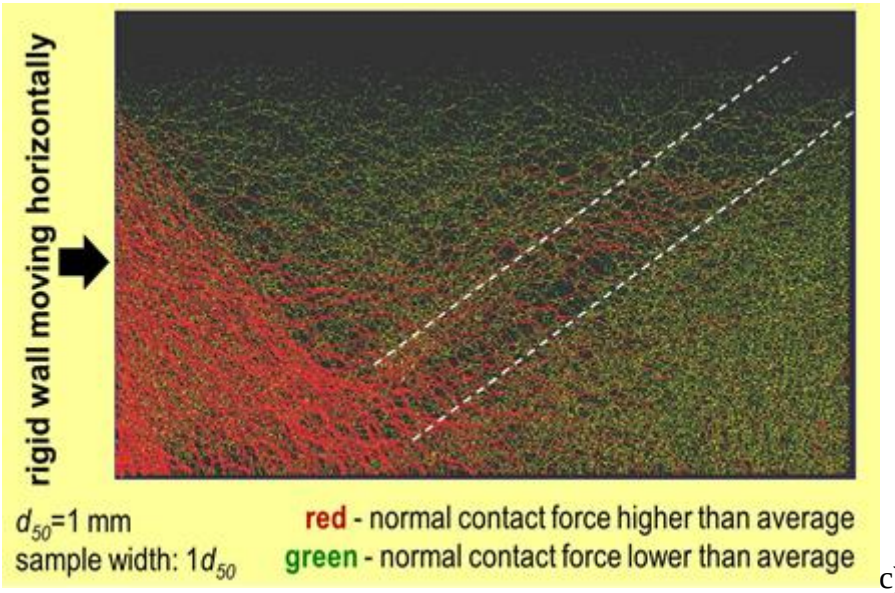

c)

A)

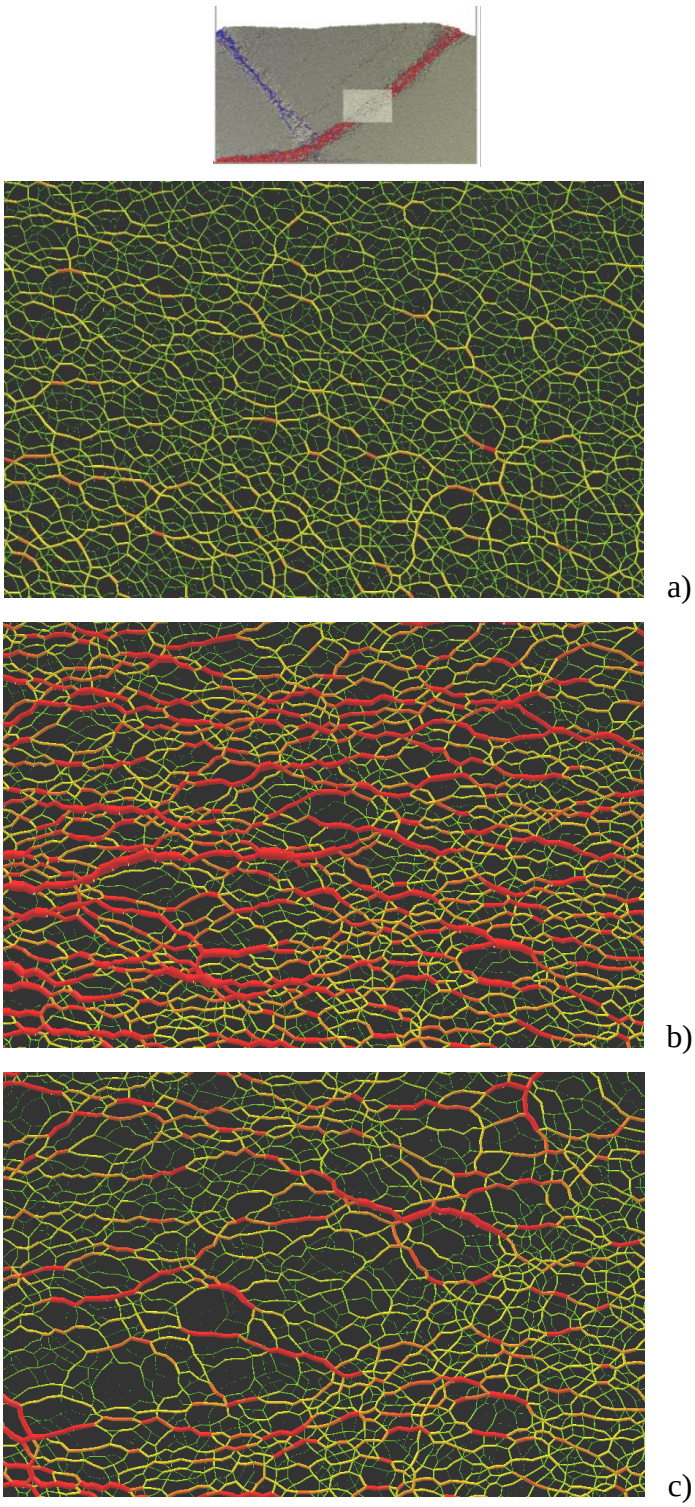

Fig. 8 DEM results (e_o = 0.62, d_{50} = 1.0mm): distribution of contact normal forces between grains in entire granular specimen for: **a** u/h = 0.02 (without shear zone), **b** u/h = 0.06 (shear zone appearance) and **c** u/h = 0.15 (full evelopment of shear zone): **A** entire granular specimen and **B** zoom on mid-region of curved shear zone (average grain displacement calculated in entire granular specimen)

The distribution of internal contact forces is non-uniform and continuously changes as it was indicated by Thornton and Zhang [29], Yan and Ji [30], Tordesillas et al. [31] and Kozicki et al. [20], Fig.8A. Force chains of heavily loaded grain contacts bear and transmit the compressive load on the entire

granular system and are the predominant structure of internal forces at micro-scale [32]. They continuously build up and collapse.

The force chains are created mainly in the region between the wall, main and radial shear zone and along the main shear zone. The loads they transmit are the highest at the triangular region adjacent to the wall (Fig.8A) - one can expect that due to a great number of strong force chains, this region acts as a quasi-rigid body (this is visible in Fig.4). Inside the main curved shear zone at the residual state, the strongest force chains are approximately perpendicular to the shear zone line (Fig.8B). The number of contacts decreases in the curved shear zone during wall translation connected to sand dilatancy (caused by the grain re-arrangement in an initially dense assembly) leading to a reduction of the number and stability of force chains (Fig.8B). At the start of deformation, the total contact number in the granular specimen was equal to 119'154 (and for the small region of Fig.8B, the contact number was 10'090). When a shear zone was initiated, this number decreased to 109'859 (8'946) at u/h=0.045. At u/h=0.09 the contact number was 108'276 (8'538), and at u/h=0.15 - 107'777 (8'038).

4.4 Distribution and evolution of displacement fluctuations

Figure 9 presents spontaneous displacement fluctuations of spheres within shear zones, having the form of cells circulating as quasi-rigid bodies (so-called vortex structures or swirls), reminiscent of turbulence in fluid dynamics [33], however the amount of the cells rotation is several ranges of magnitude smaller (~0.01^o-0.1^o) then fluid vortex rotation. Similar rotational structures were observed both in quasi-static experiments [4]-[6] and DEM simulations [33]-[38]. It is usually expected that this non-uniform rotational micro-structure is directly related to buckling of force chains. The existence of vortices during granular flow is still unexplained. The plots in Fig.9 were obtained by drawing the difference $\vec{V}_i - \vec{V}_{avr}$ between the displacement vector for each sphere and the average background translation corresponding to the homogeneous (affine) strain in the entire specimen ($\vec{V}_i$ represents the increment of sphere displacement and $\vec{V}_{avr}$ is the average background displacement of spheres in the entire granular specimen during e.g. n=1000 iterations). The individual particle displacements are able to form long-range deformation vortex structures which rotate as rigid bodies while the space between them is under intense shear deformation. The vortex-like patterns are well recognized in the main curved shear zone, in particular, at the residual state for the highest mean grain diameter d_{50}=5 mm (Fig.9a). Several clockwise rotating vortices: e.g. 3 for d_{50}=5 mm and 10 for d_{50}=1 mm occur along the shear zone, having the diameter of about the shear zone width t_s. The distance between the vortices is

variable – some of them are close to each other (at about t_s distance) or far away from each other (at the distance of about $5\times t_s$). The vortex structures are well visible in the main curved shear zone if the number of iterations n is high enough, i.e. $n\geq 1000$ ($u/h\geq 0.001$) (Fig.10). The evolution of displacement fluctuations at the residual state during deformation $\Delta u/h=0.01$ (n=1'000) demonstrates that vortex structures have a tendency to appear and disappear intermittently in the course of deformation (Fig.11). Note that the vectors in Figs.10 and 11 (which are solely ≈0.1 mm long on average) are multiplied by the factor 50-300. Therefore some wild vectors sometimes appear.

A) B)

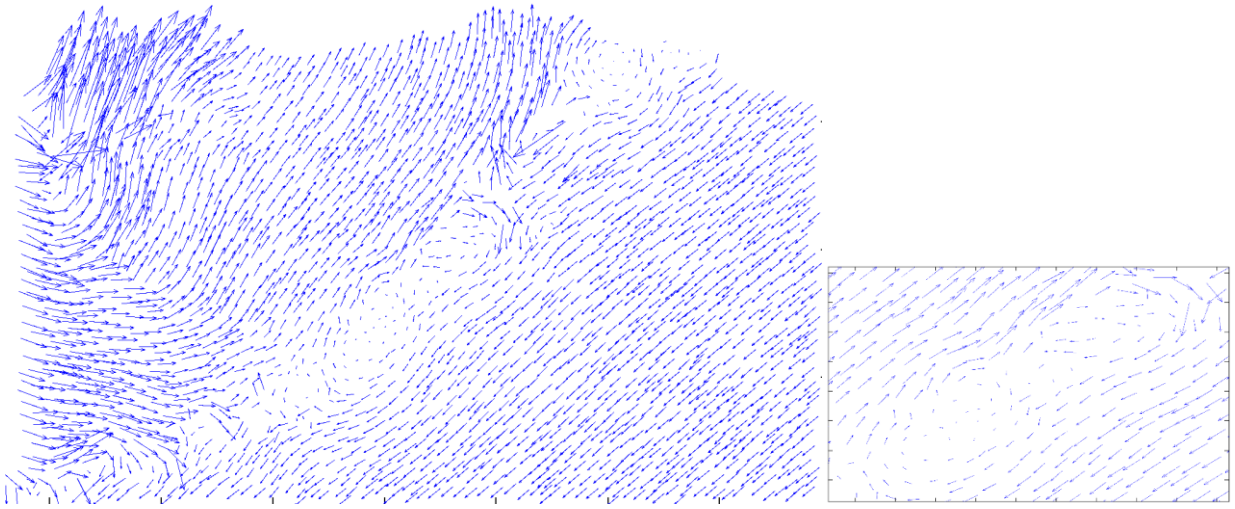

a)

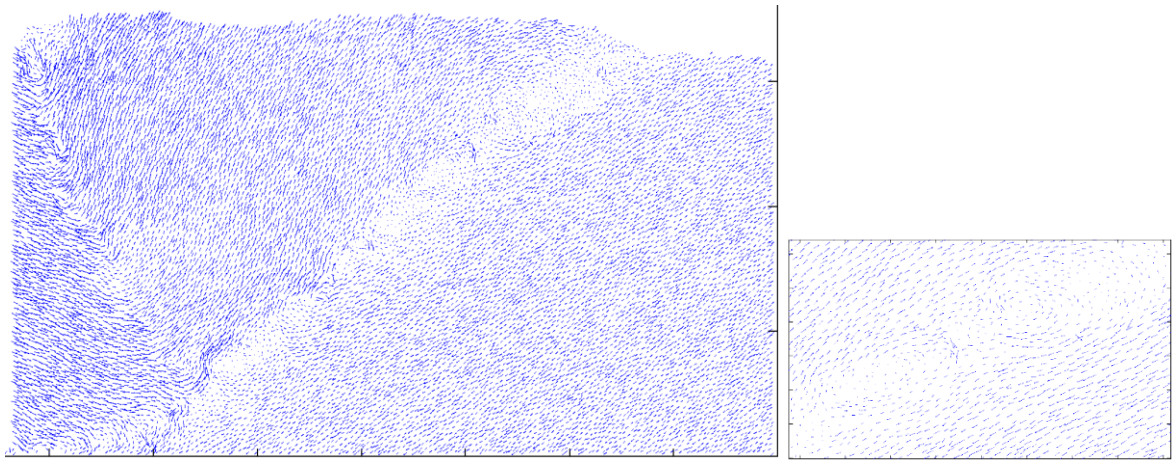

b)

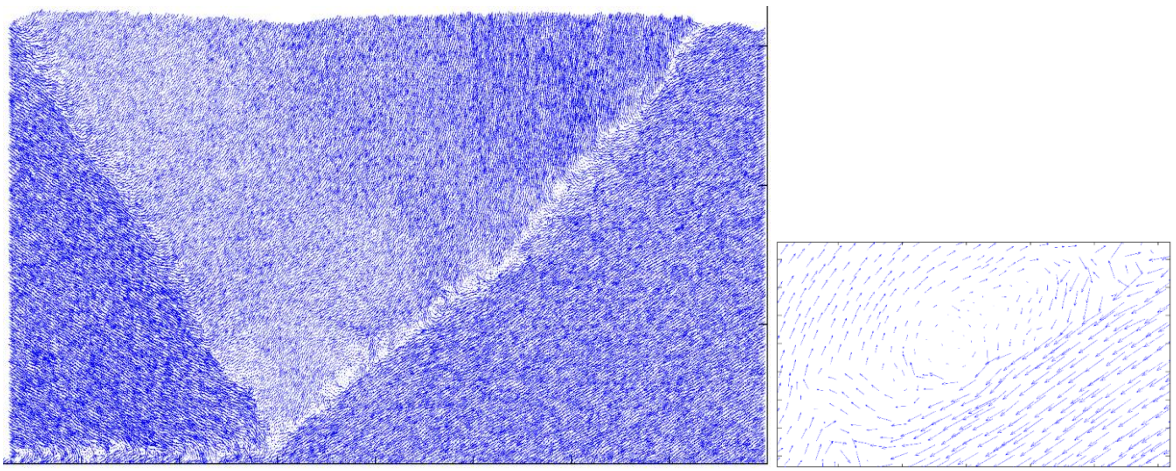

c)

Fig. 9 DEM results (e_o = 0.62) for displacement fluctuation vectors in form of vortex structures at residual state of u/h = 0.15 for different mean grain diameter: **a** d_{50} = 5 mm, **b** d_{50} = 2mm and **c** d_{50} = 1.0 mm,
A entire granular specimen,
B zoom of mid-region of curved shear zone
(n = 1000-iteration number when grain displacement increment vectors are calculated, average grain displacement is calculated in entire granular specimen, vectors are magnified by factor 50)

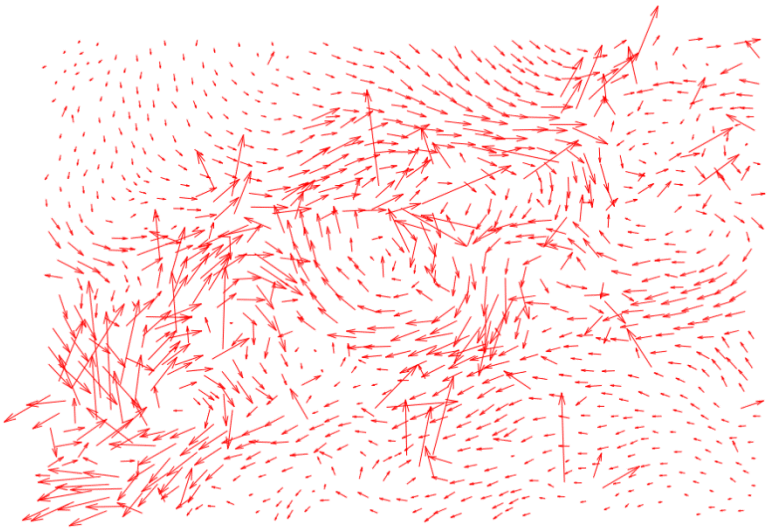

a)

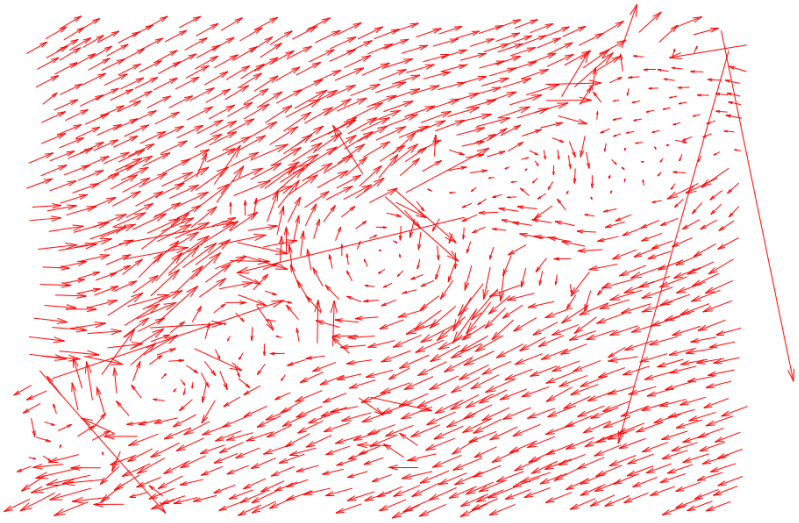

b)

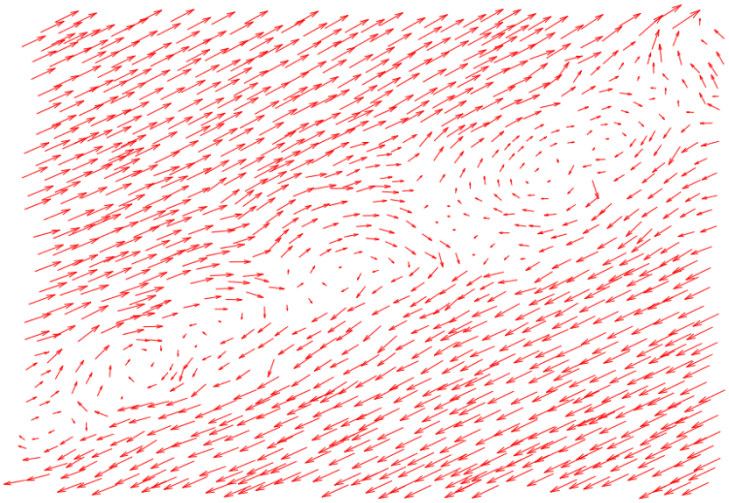

c)

Fig. 10 DEM results (e_o = 0.62, d_{50} = 5mm) for evolution of displacement fluctuation vectors in mid-region of curved shear zone at residual state of u/h = 0.15 for different iteration number n: **a** n = 100, **b** n = 1000 and **c** n = 10,000 (average grain displacement is calculated in entire granular specimen, vectors are magnified by factor 500, 50 and 10, respectively)

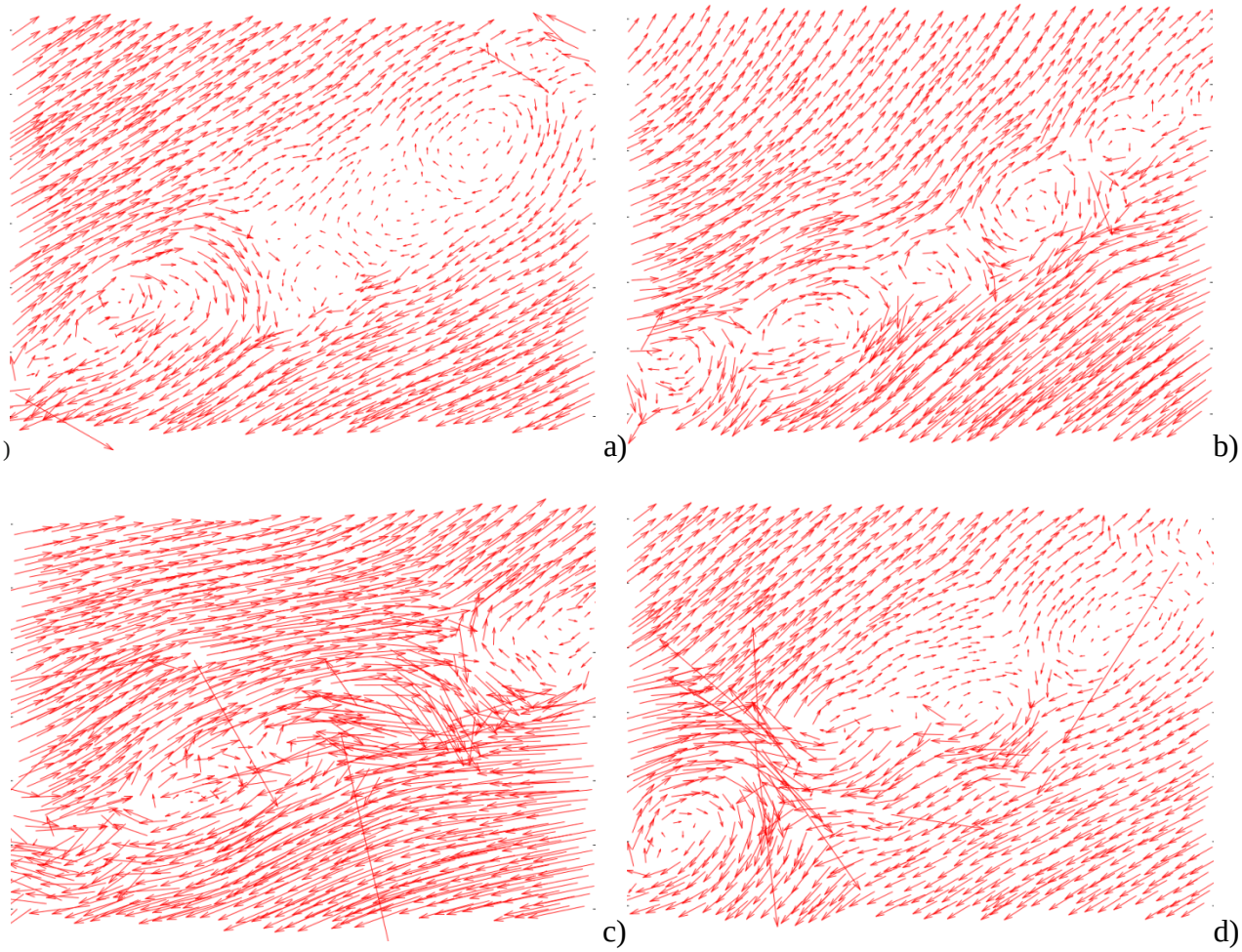

) a) b)

c) d)

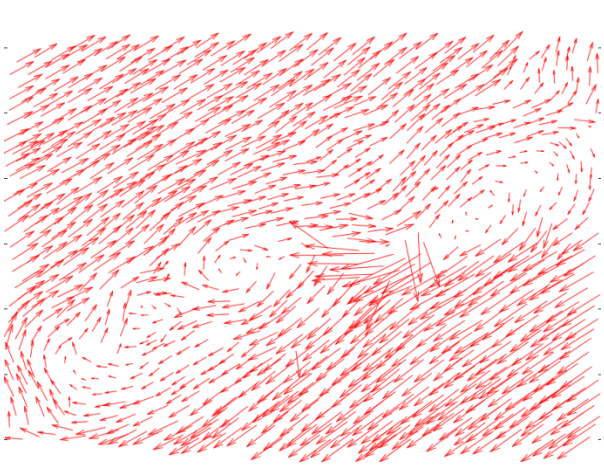

e)

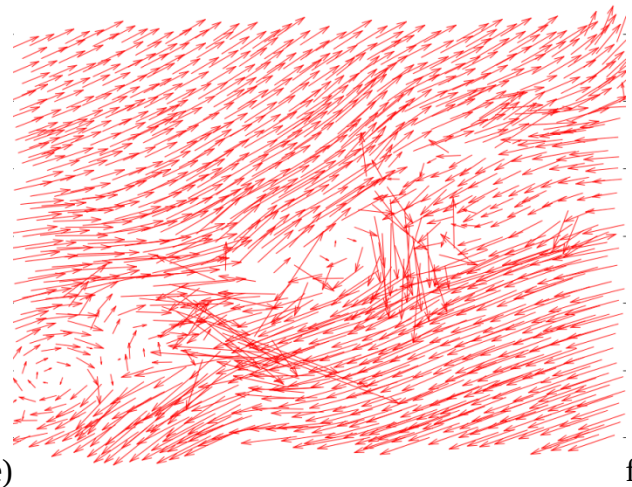

f)

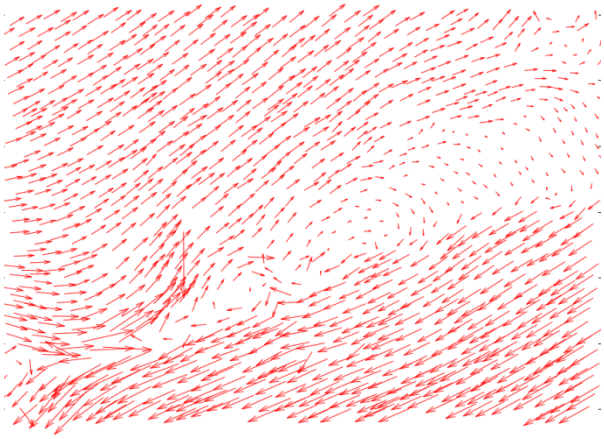

g)

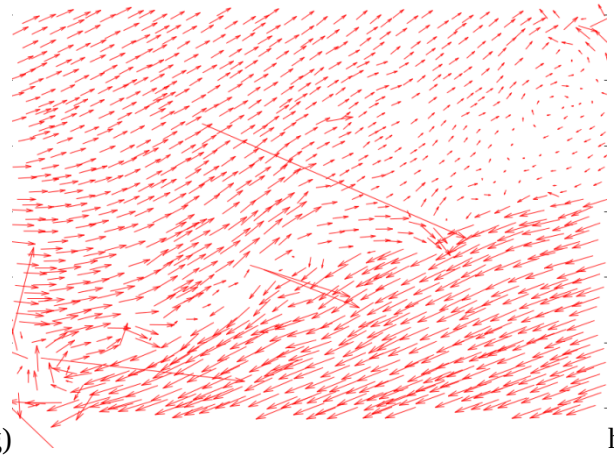

h)

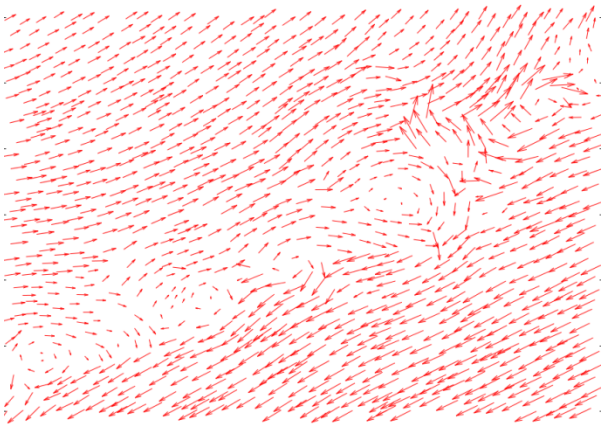

i)

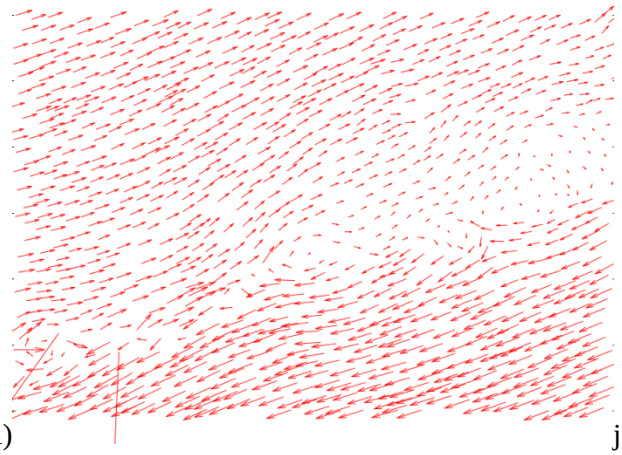

j)

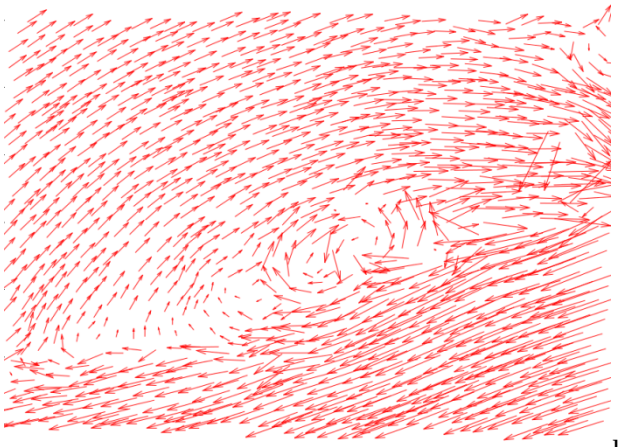

k)

Fig. 11 DEM results (e_o = 0.62, d_{50} = 5mm) for evolution of displacement fluctuation vectors (stages **a**–**k**) in mid-region of curved shear zone at residual state at u/h = 0.15–0.17 (n = 1000, average grain displacement is calculated in entire granular specimen, vectors are magnified by factor 50)

The vortices were not observed along the radial shear zone because of an insufficient magnitude of displacements within this zone. If the average background translation is limited to the region of e.g. A_s=2t_s × 2t_s (i.e. 2×20d_{50}=40 mm), the vortices are also observable in the radial zone (Fig.12). For the spheres with d_{50}=5 mm, 7 vortex-structures occur in the curved shear zone and 3 in the radial shear zone (Fig.12a), and with d_{50}=1 mm, 16 vortex-structures happen in the curved shear zone and 7 in the radial shear zone (Fig.12b)

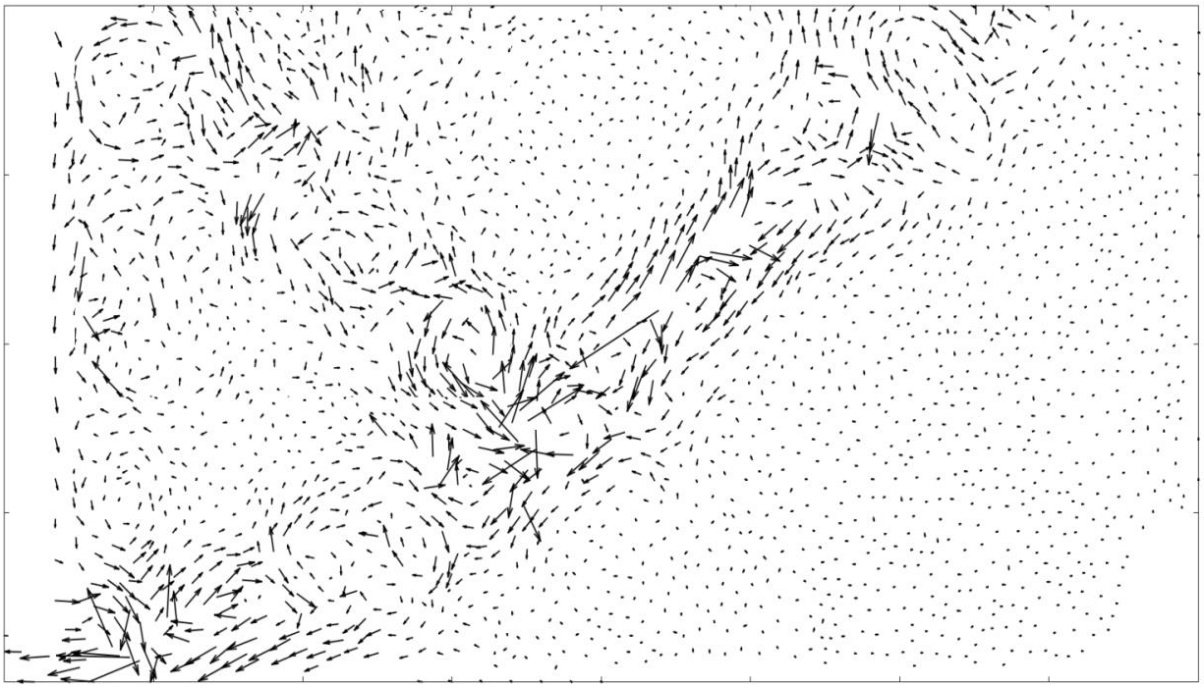

a)

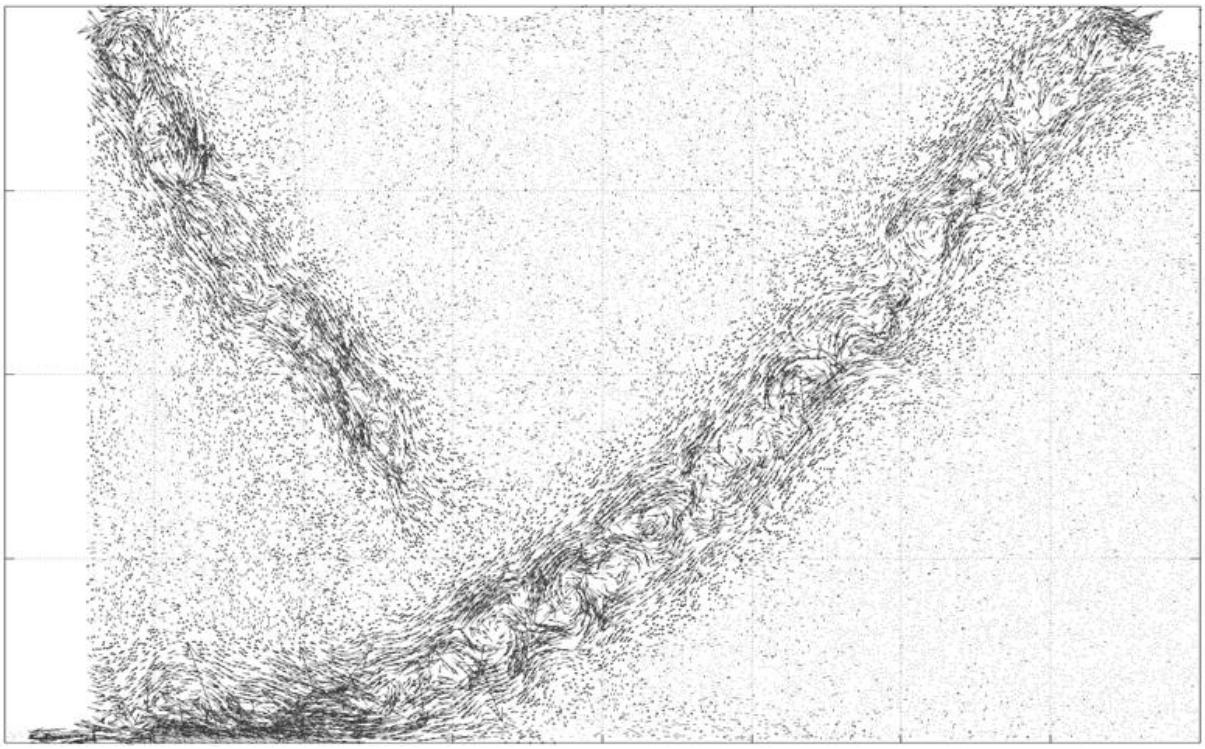

b)

Fig. 12 DEM results (e_o = 0.62) for displacement fluctuation vectors in form of vortex structures at residual state of u/h = 0.15: **a** d_{50} = 5.0mm and **b** d_{50} = 1.0mm (average grain displacement is calculated for area $As = 2t_s \times 2t_s$ (i.e. $2 \times 20d_{50}$ = 40 mm, vectors are magnified by factor 100)

A direct link between force chains, vortex structures and void ratio changes in the region 70×100 mm^2 of the main curved shear zone at the residual state, during the wall normalized displacement interval of u/h=0.01 (from u/h=0.15 up to u/h=0.16) is demonstrated in Fig.13 for the granular specimen built of d_{50}=5 mm spheres (the average background translation is calculated in the entire granular specimen). Two deformation stages are considered: 1) when the vortex exists at u/h=0.15 (Fig.13Aa) and 2) when the vortex does not exist at u/h=0.16 (Fig.13Ba). The force chain vanishes at u/h=0.15 (Fig.13Ba) and the new force chain is created at u/h=0.16 (Fig.13Bb). Small local dilatancy occurs close to a broken force chain (Figs.13Bc, e) and small local contractancy takes place near a new force chain (Figs.13Bd, e). Thus, the occurrence and vanishing of vortex structures is related to the force chain creation and disappearance and to the void ratio decrease and increase [21], respectively.

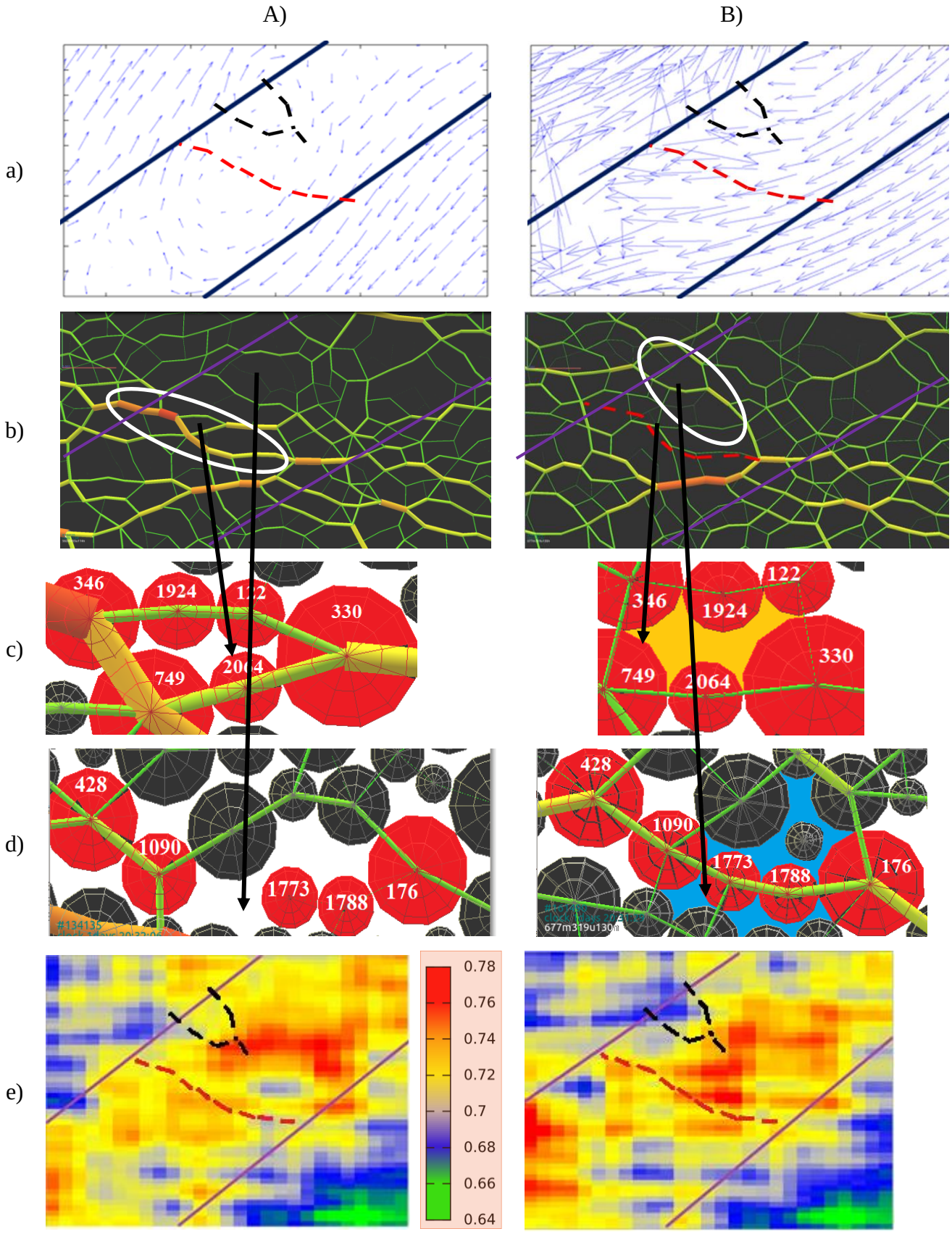

Fig. 13 DEM results (e_o = 0.62, d_{50} = 5mm) for evolution of microstructure in main curved shear zone for normalized wall displacement at u/h = 0.15 (**A**) and u/h = 0.16 (**B**) (*solid lines* shear zone edges):
a map of displacement fluctuations of Fig. 8Ba (*red dashed line* broken force chain, *black dashed line* new force chain), **b** geometry of force chains between grains (*red dashed line* broken force chain), **c**, **d** zoom on geometry of force chains and grains (*red grains* build force chain, *yellow colour between grains* denotes higher void ratio, *blue colour* between

grains denotes lower void ratio) and **d** map of void ratio with intensity scale (*red colour* corresponds to higher void ratio, *red dashed line* bro ken force chain, *black dashed line* new force chain), *n* = 1000-iteration number when calculating grain displacement fluctuation vectors (with average grain displacement calculated in entire granular specimen)

Figure 14 shows the evolution of displacement fluctuations and rotations of five single spheres (d_{50}=5 mm) selected for observations within the granular curved shear zone and numbered from '1' to '5'. The period between the wall normalized translation–u/h=0.2 and u/h=0.5 was inspected. The spheres '1-5' were placed inside the vortex which was created at u/h=0.2 (Fig.14C). The displacement fluctuation vectors for spheres '1-5' are small in the vortex and become larger when the vortex vanishes due to shearing (Figs.14A and 14C). The vortex appearance is related to a high (sphere '1') or a small fold (spheres '2-5') of sphere displacement fluctuation vectors (Fig.14A). The vortex is not always created by the same spheres (Fig.14C). The sphere rotations inside a vortex are insignificant (spheres '1-5' in Fig.14B). They may increase when a vortex vanishes due to intense shearing (spheres '1', '4' and '5' in Fig.14B).

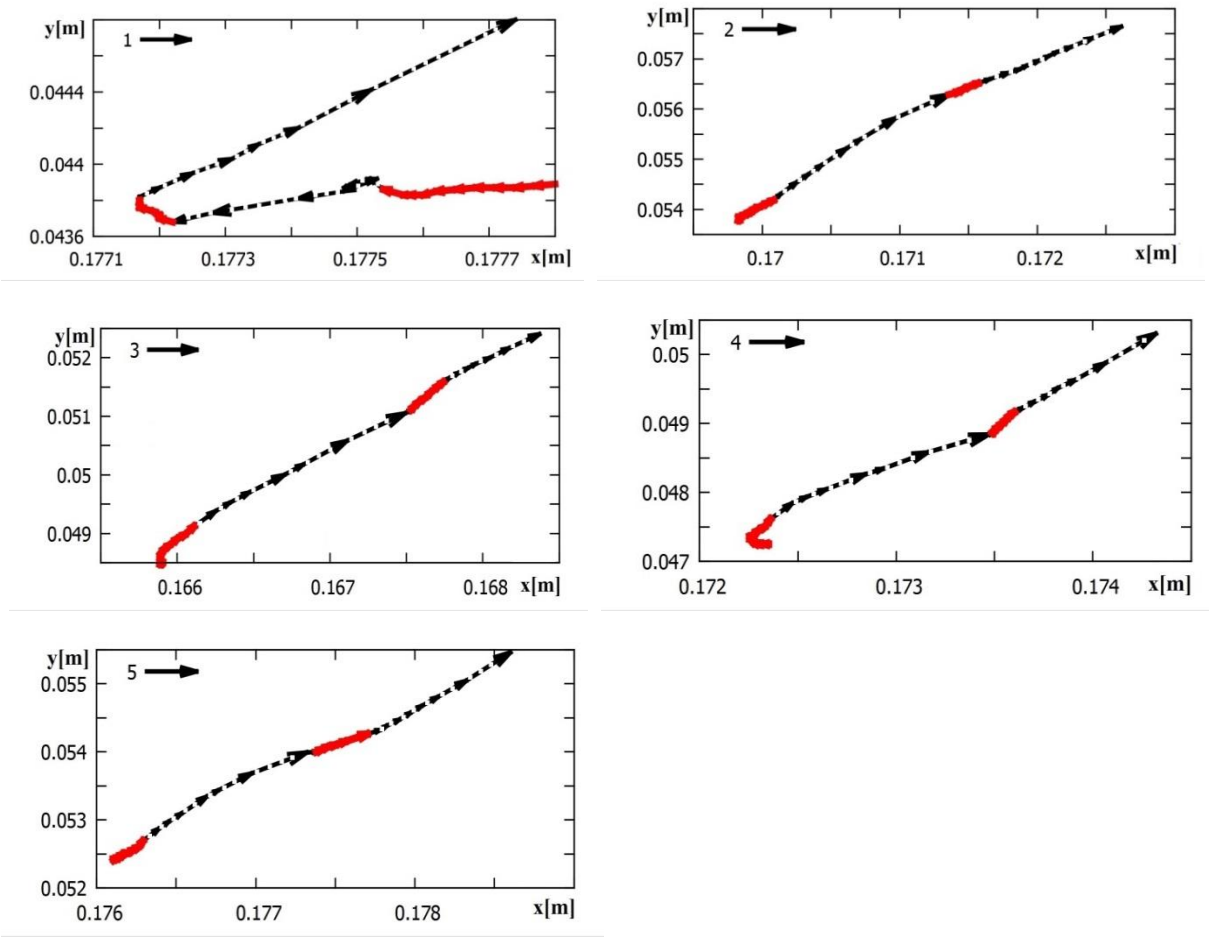

A)

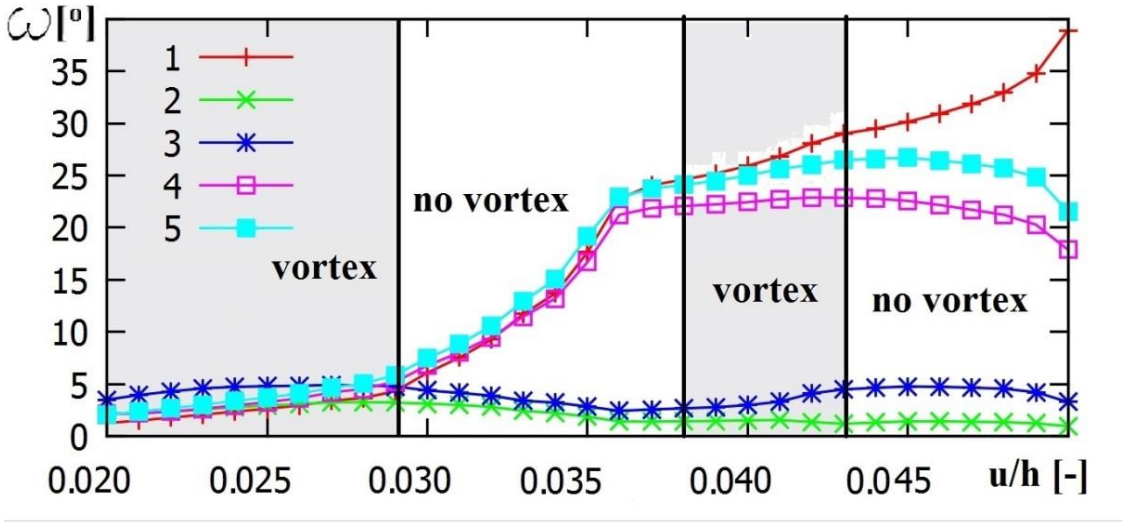

B)

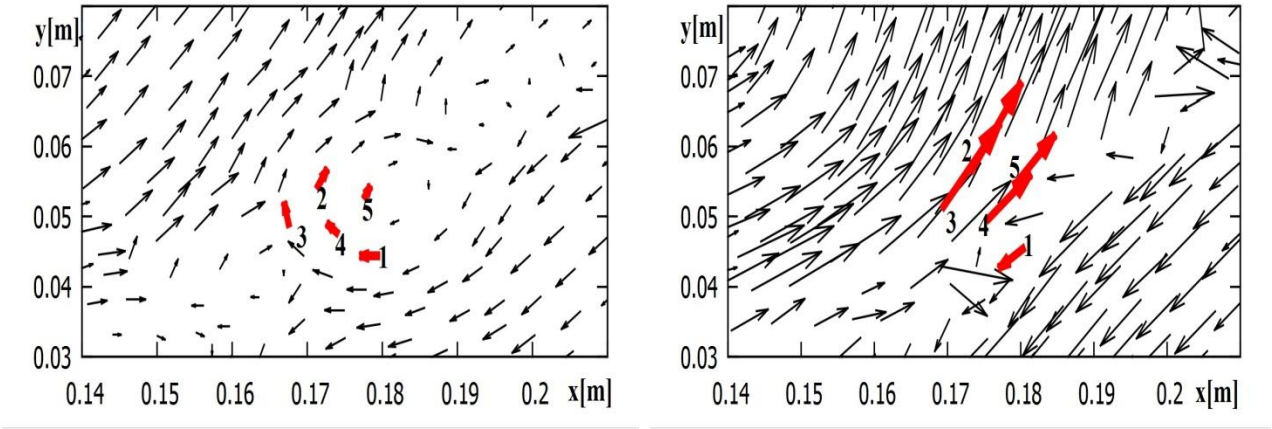

a) b)

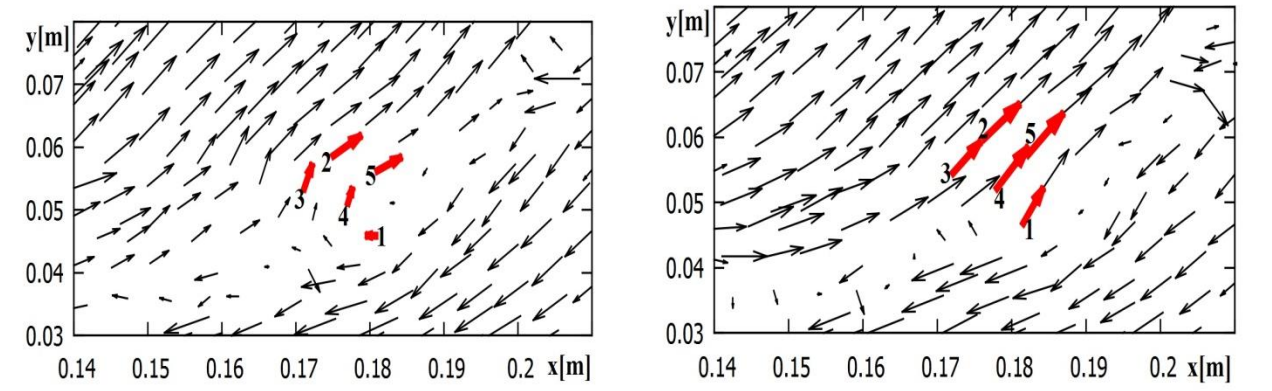

c) d)

Fig. 14 DEM results (e_o = 0.62, d_{50} = 5mm) for evolution of dis placement fluctuation vectors (*solid red arrows* vortex exists, *dotted black arrows* vortex does not exist) (**A**) and rotations ω (**B**) of single grains '1–5' between normalized wall translation u/h = 0.02 and u/h = 0.05 during appearance and disappearance of vortex structures in main curved shear zone (**C**): **a** u/h = 0.025, **b** u/h = 0.035, **c** u/h = 0.042 and d) u/h = 0.049 (n = 1000-iteration number, average grain displacement is calculated in entire granular specimen)

Finally, the frequency of the vortex appearance based on displacement fluctuations of spheres in a curved shear zone is presented in Fig.15 (for d_{50}=5 mm). The sphere displacements are averaged over the cell area $A_s=5d_{50}\times5d_{50}$ and the average background translation is again calculated from the entire specimen. In order to mathematically describe vortices, the displacement fluctuation vector of each sphere (green spheres) in the neighbourhood of each central sphere (blue sphere) is decomposed into 2 vectors: the normal and tangential to the movement direction of each central sphere (Fig.15a). Only the tangential displacement fluctuations are assumed to be responsible for a vortex, i.e. if the neighbouring spheres had solely the tangential displacement fluctuation component, the central blue sphere (the blue one in Fig.15b) is assumed to be located in a vortex mid-point. In order to avoid the prescribing pure shearing along a shear zone as a vortex, a certain limitation is imposed, i.e. the condition that the sum of the tangential displacement fluctuations has be at least twice as big as the sum of the normal displacement fluctuations (to be classified as a part of the vortex). The location of vortices based on the displacement fluctuation field in the granular specimen is presented in Fig.15c, wherein the blue circles correspond to the vortices (more circles at the same place indicate a larger vortex, and ~~a~~ larger circles denote ~~a~~ more regular vortex). The displacement fluctuation vector field shown in Fig.15c is similar to the one from Fig.8Aa. Figure 15d shows the frequency (expressed in the relative displacement *u/h* value) of one arbitrary selected vortex from the curved shear zone (marked with the green rectangle in Fig.15c). The high value of *S* (*S* - the sum of the tangential displacement fluctuation vectors) characterizes a more pronounced vortex and *S*=0 corresponds to its disappearance. The sum of the tangential displacement fluctuation *S* strongly varies during deformation (Fig.15d). The strong vortex (e.g. *S*>0.8 mm in Fig.15d) appeared in the curved shear zone 2 times for *u/h*=0.06-0.08, the medium-strong (e.g. 0.4≤*S*≤0.8 mm) 7 times every *u/h*=0.01-0.02 and the weak one (e.g. *S*<0.4 mm) 18 times every *u/h*=0.002-0.03. The vortex appears when a shear zone has been already created. Its intensity is lower in the residual state (*u/h*>0.10). The predominant period of the vortex is equal to 3% and 5% of *u/h* using the Fourier transformation (Fig.15e). In the case of the average background translation calculated from the cell area of $A_s=2t_s \times 2t_s$, the sum *S* is higher (Fig.16a). The strong vortex (S > 0.8mm) occurs again 2 times for *u/h*=0.06-0.08, the medium-strong vortex ($0.4 \le S \le 0.8$ mm) 5 times every *u/h*=0.002-0.03 and the weak one (*S*< 0.4 mm) 20 times every *u/h*=0.001-0.02. The predominant period of the vortices with respect to *u/h* is similar and equal to 5% (Fig.16c).

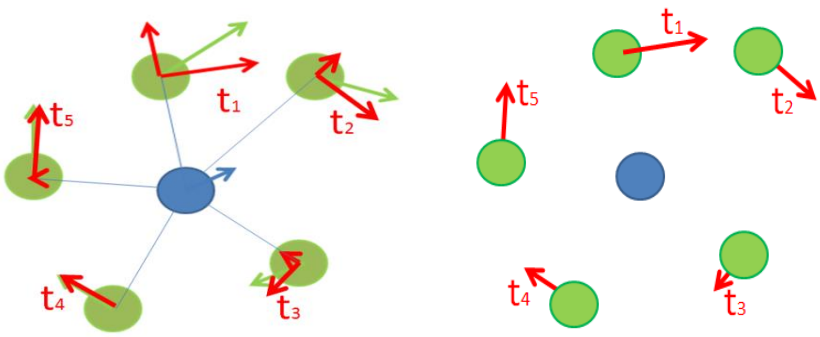

a) b)

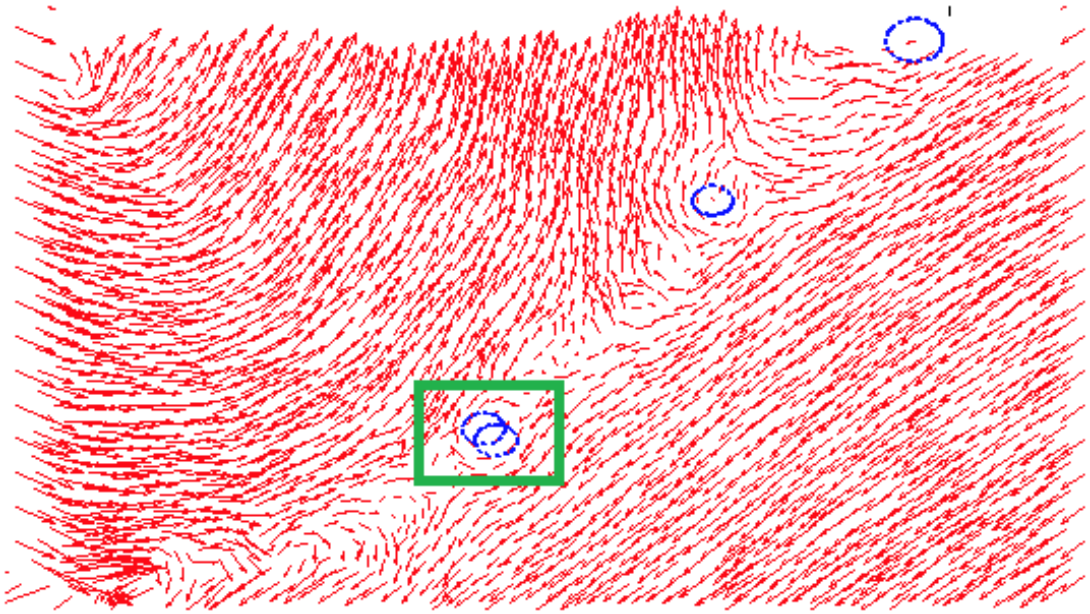

c)

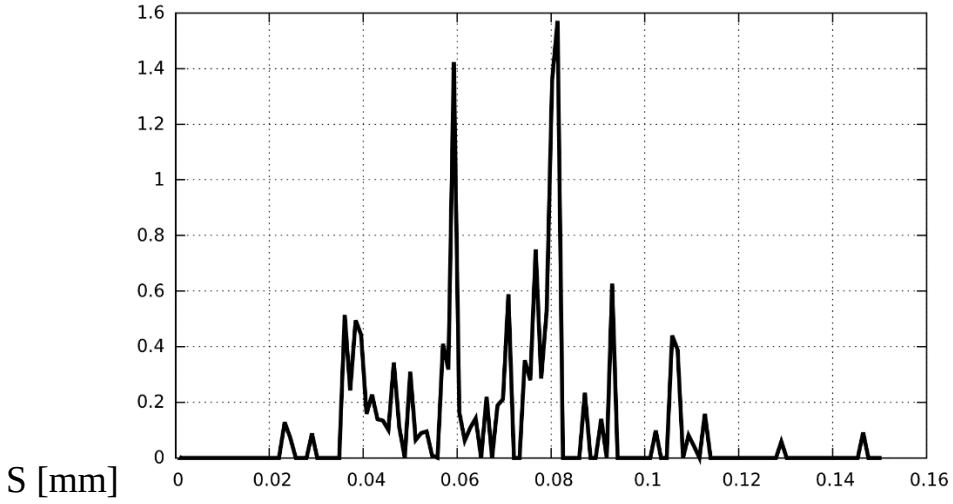

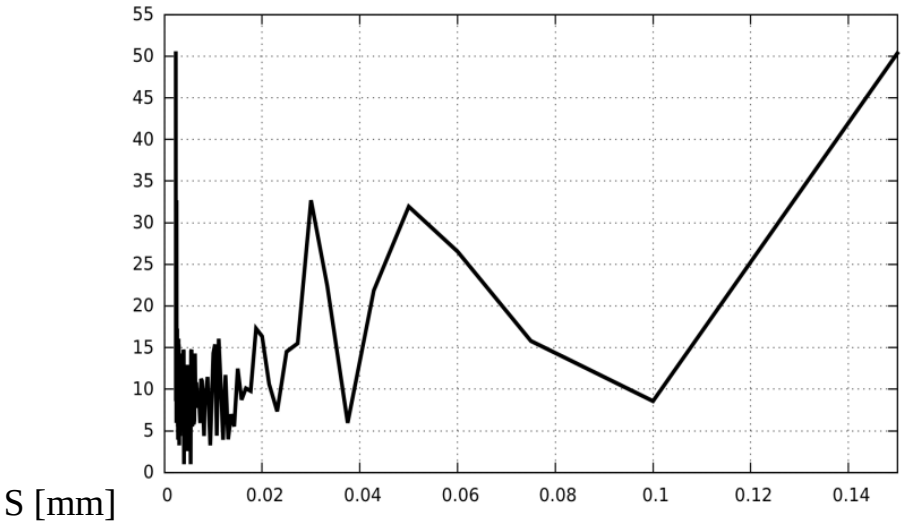

Fig. 15 DEM results (e_o = 0.62, d_{50} = 5mm) for one vortex within curved shear zone: **a** tangential and normal displacement fluctuation vectors of single grains with respect to central grain movement, **b** displacement fluctuation vectors creating vortex, **c** field of single grain displacement fluctuation with marked vortices and **d** frequency of selected single vortex during deformation expressed in u/h (S - the sum of tangential displacement fluctuation vectors over the area $As = 5d_{50} \times 5d_{50}$) and **e** S-value against vortex period with respect to normalized wall translation u/h (average background translation is calculated for entire specimen)

Summarizing, the DEM simulation results of the small-scale earth pressure problem show good qualitative agreement to the experimental findings. More realistic calibration of the DEM is possible based on experiments using DIC (to compare strains and volume changes within shear zones) and photo-elastic technique (to compare the structure of contact forces) [3].

The DEM results show that the conventional earth pressure mechanisms with slip surfaces [24] are roughly reproduced. The actual internal friction angle within shear zones at peak (φ^p) cannot be known in advance since it depends strongly on the initial and boundary conditions of the entire system. Therefore, it is difficult to obtain realistic earth pressures with a conventional earth pressure theory. In addition, the different friction angles are mobilized in various shear zones at the same time and the varying friction angle values occur also along the same shear zone. The micro-structural events cause that the distribution of global quantities such void ratio is strongly non-uniform and the resultant earth pressure strongly force oscillates.

The results of discrete simulations will contribute to calibrate better a micro-polar hypoplastic constitutive model [39], [40] with respect to micro-polar terms that requires an accurate description of the micro-scale kinematics within shear zones. In turn, the knowledge on vortex-force chain correlations allows for introducing stress fluctuations (connected to a build-up and collapse of force chains) more realistically into a hypoplastic constitutive model.

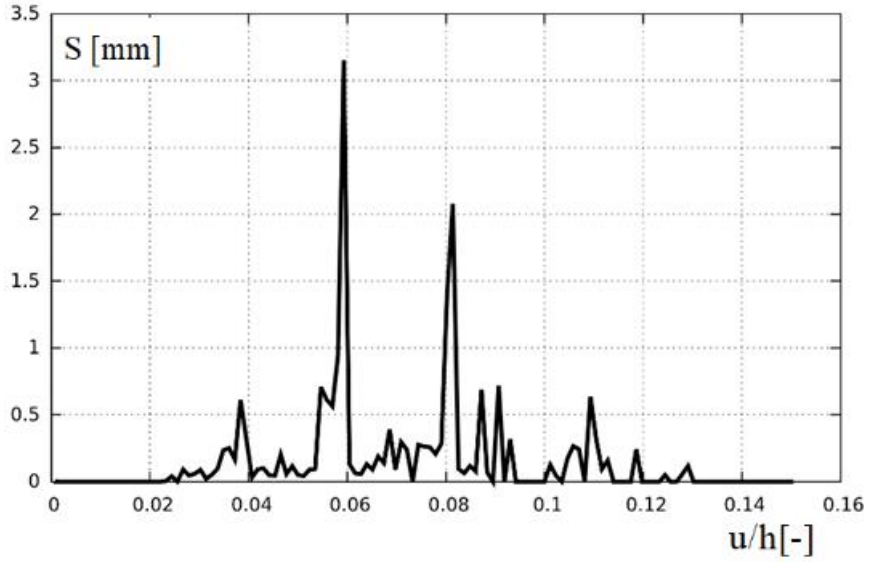

a)

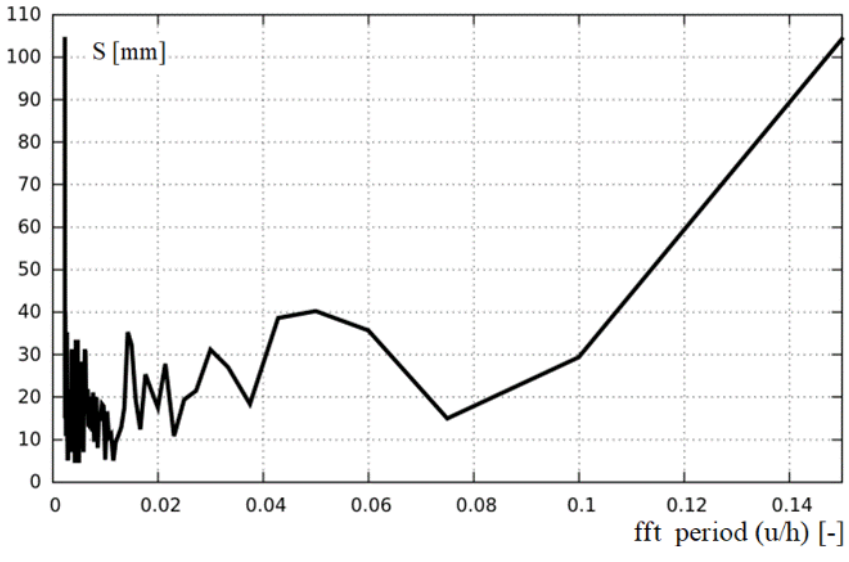

Fig. 16 DEM results (e_o = 0.62, d_{50} = 5mm) for one vortex within curved shear zone: **a** frequency of selected single vortex during deformation expressed in u/h (S - the sum of tangential displacement fluctuation vectors over the area As = $5d_{50} \times 5d_{50}$) and **b** S-value against vortex period with respect to normalized wall translation u/h (average background translation is calculated for area $As = 2t_s \times 2t_s$)

5. Conclusions

The following conclusions can be drawn from our discrete DEM simulations of passive earth pressures problem:

• DEM realistically simulates a complex experimental pattern of shear zones and can be used in the future research to study the build-up of the passive earth pressure from the at rest condition. Grain rotations are noticeable only within shear zones. The global wall pressure, thickness of the main shear zones and the earth pressure oscillations increase with growing mean grain size. The thickness increases from $20d_{50}$ (d_{50}=1 mm) up to $10d_{50}$ (d_{50}=5 mm). The number of the secondary radial shear zones increased with d_{50} for the same normalized wall translation at the residual state.

• The distribution of internal contact forces is non-uniform due to a build-up and collapse of force chains. The number of contact forces continuously decreases in a granular specimen with material dilatancy.

• Vortex structures and local void ratio fluctuations spontaneously appear within displacement field of shear zones and seem to have periodically organized structure. The diameter of vortex corresponds to the shear zone thickness. The number of vortices increases with decreasing mean grain diameter and the distance between them increases with increasing mean grain diameter. They appear with different intensity and frequency. The vortices move as rigid bodies with small displacement fluctuations and

insignificant rotations of single spheres. They seem to be a manifestation of grain rearrangement as the amount of their rotation is very small. If the average background translation is calculated from the smaller area, the number of vortices increases (the predominant period is similar).

• The deformation of force chains plays a key role in the formation of vortex structures. The vanishing and appearing of vortices may be connected not only to the collapse and build-up of force chains but also to their deformation. The collapse of force chains leads also to the formation of larger voids and their build-up to the formation of smaller voids.

Acknowledgements

The research work has been carried out as a part of the Project 2011/03/B/ST8/05865 "*Experimental and theoretical investigations of micro-structural phenomena inside strain localization in granular materials*" financed by Polish National Research Centre (NCN) in the time period 2013-2015. The project was approved in the end of 2012 by the review board of Polish National Research Centre.

References

[1] Roscoe, K.H. The influence of strains in soil mechanics. Geotechnique 20, 2, 129-170, 1970.

[2] Widulinski, L., Tejchman, J., Kozicki, J., Leśniewska, D. Discrete simulations of shear zone patterning in sand in earth pressure problems of a retaining wall. Int. Journal of Solids and Structures 48, 7-8, 1191-1209, 2011.

[3] Leśniewska, D., Niedostatkiewicz, M., Tejchman, J. Experimental study on shear localization in granular materials within combined strain and stress field. Strain 47, 2, 218-231, 2012.

[4] Abedi, S., Rechenmacher, A.L., Orlando, A.D. Vortex formation and dissolution in sheared sands. Granular Matter 14, 6, 695-705, 2012.

[5] Richefeu, V., Combe, G., Viggiani, G. An experimental assessment of displacement fluctuations in a 2D granular material subjected to shear. Geotechnique Letters 2, 113–118, 2012.

[6] Miller, T, Rognon, P, Metzger, B, et al. Eddy viscosity in dense granular flows. Phys Rev Letters 111(5):058002, 2013.

[7] Lucia, J.B.A. Passive earth pressure and failure in sand. Research Report, University of Cambridge, 1966.

[8] Gudehus, G., Schwing, E. Standsicherheit historischer Stützwände. Internal Report of the Institute of Soil and Rock Mechanics, University Karlsruhe, 1986.

[9] Niedostatkiewicz, M., Leśniewska, D., Tejchman, J. Experimental analysis of shear zone patterns in sand for earth pressure problems using Particle Image Velocimetry. Strain, 47, s2, 218-231, 2011.
[10] Cundall, P.A., Hart, R. Numerical modeling of discontinua. J. Eng. Comp. 9, 101–113, 1992.
[11] Šmilauer, V., Chareyre, B. Yade DEM Formulation. Manual, 2011.
[12] Kozicki, J., Donze, F.V. A new open-source software developed for numerical simulations using discrete modelling methods. Computer Methods in Applied Mechanics and Engineering 197, 4429-4443, 2008.
[13] Iwashita, K., Oda, M. Rolling resistance at contacts in simulation of shear band development by DEM. ASCE J Eng Mech, 124(3), 285-92, 1988.
[14] Jiang, M.J., Yu, H-S., Harris, D. A novel discrete model for granular material incorporating rolling resistance. Computers and Geotechnics 32, 340-357, 2005.
[15] Mohamed, A., Gutierrez, M. Comprehensive study of the effects of rolling resistance on the stress-strain and strain localization behaviour of granular materials. Granular Matter 12, 5, 527-541, 2010.
[16] Kozicki, J., Tejchman, J., Műhlhaus, H.-B. Discrete simulations of a triaxial compression test for sand by DEM. International Journal for Analytical and Numerical Methods in Geomechanics, 38, 1923-1952, 2014.
[17] Kozicki, J., Tejchman, J., Mróz, Z. Effect of grain roughness on strength, volume changes, elastic and dissipated energies during quasi-static homogeneous triaxial compression using DEM. Granular Matter 14, 4, 457-468, 2012.
[18] Hertz, H. 1882. On the contact of elastic solids. J. Reine und Angewandte Mathematik 92, 156-171, 1982.
[19] Mindlin, R. D. and Deresiewicz, H. Elastic spheres in contact under varying oblique forces. J. Appl. Mech. Trans. A.S.M.E. 75, 327-344, 1953.
[20] Kozicki, J., Niedostatkiewicz, M., Tejchman, J., Mühlhaus, H.-B. Discrete modelling results of a direct shear test for granular materials versus FE results. Granular Matter 15, 5, 607-627, 2013.
[21] Wu, W. Hypoplastizität als mathematisches Modell zum mechanischen Verhalten granularer Stoffe (in German). Heft 129, Institute for Soil- and Rock-Mechanics, University of Karlsruhe, 1992.
[22] Goldhirsch, I. Rapid granular flows. Annu. Rev. Fluid Mech. 35, 267-293, 2003.
[23] Roux, J.N., Chevoir, F. Discrete numerical simulation and the mechanical behaviour of granular materials. Bulletin des Laboratoires des Ponts et Chaussees 254, 109-138, 2005.
[24] Gudehus, G., Nübel, K. Evolution of shear bands in sand. Geotechnique 113, 54 (3), 187–201, 2004.
[25] Tejchman, J., Bauer, E., Tantono, S.F. Influence of initial density of cohesionless soil on evolution of passive earth pressure. Acta Geotechnica 2, 1, 53-63, 2007.

[26] Tejchman, J. FE modeling of shear localization in granular bodies with micro-polar hypoplasticity. Springer Series in Geomechanics and Geoengineering (eds. Wu and Borja), Springer Verlag, Berlin-Heidelberg, 2008.

[27] Gudehus, G. Erddruckermittlung. Grundbautaschenbuch, Teil 1, Ernst und Sohn, 1996.

[28] Chupin, O, Rechenmacher, A.L and Abedi, S. Finite strain analysis of non-uniform deformations inside shear bands in sands. International Journal for Numerical and Analytical Methods in Geomechanics, 1651-1666, 2012.

[29] Thornton, C., Zhang, L. Numerical simulations of the direct shear test. Chemical Engineering Technology, 26(2), 1-4, 2003.

[30] Yan, Y., Ji, S. Discrete element modelling of direct shear test for a granular material. Int. Journal of Numerical and Anal. Methods in Geomechanics 34, 978-990, 2010.

[31] Tordesillas, A., Walker, D. M., Qun Lin, Q. 2010. Force cycles and force chains. Physical Review E 81, 011302.

[32] Muir Wood, D. and Lesniewska, D. Stresses in granular materials. Granular Matter 13, 395–415, 2011.

[33] Radjai, F., Roux, S. Turbulent-like fluctuation in quasi-static flow of granular media. Phys. Rev. Lett. 89, 064302, 2002.

[34] Kuhn, M.R. Structured deformation in granular materials. Mechanics of Materials 31, 407-442, 1999.

[35] Alonso-Marroquin, F., Vardoulakis, I and Herrmann, H., Weatherley, D. and Mora, P. Effect of rolling on dissipation in fault gouges. *Physical Review E* 74, 031306, 1-10 (2006).

[36] Liu, X., Papon, A., Mühlhaus, H.-B. Numerical study of structural evolution in shear band. Philosophical Magazine 92, 28-30, 3501-3519, 2012.

[37] Peters, J.F, Walizer, L.E. Patterned nonaffine motion in granular media**.** Journal of Engineering Mechanics 139, 10, 1479-1490, 2013.

[38] Tordesillas, A., Muthuswamy, M., Walsh, S.D.C. Mesoscale measures of nonaffine deformation in dense granular assemblies. Journal of Engineering Mechanics 134(12):1095-1113, 2008.

[39] Tejchman, J., Górski, J. Computations of size effects in granular bodies within micro-polar hypoplasticity during plane strain compression. Int. Journal for Solids and Structures 45, 6, 1546-1569, 2008.

[40] Tejchman, J. Wu, W. Modeling of textural anisotropy in granular materials with stochastic micro-polar hypoplasticity. Int. Journal of Non-Linear Mechanics 42, 6, 882-894, 2007.